

Evolution of jets emanating from short holes into crossflow

By **S. D. PETERSON** AND **M. W. PLESNIAK**

School of Mechanical Engineering, Maurice J. Zucrow Laboratory, Purdue University,
West Lafayette, IN, 47907-1003, USA
plesniak@ecn.purdue.edu

(Received 20 May 2002 and in revised form 15 September 2003)

The evolution of a short injection-hole jet issuing into a crossflow at low blowing ratios is presented. Particle image velocimetry (PIV) is used to determine structural features of the jet/crossflow interaction throughout its development from within the jet supply channel (which feeds the holes), through the injection hole, and into the crossflow. The effect of supply channel feed orientations, i.e. counter to, or in the same direction as the crossflow is emphasized. Feed orientation profoundly affects such jet characteristics as trajectory and lateral spreading, as well as its structural features. Fluid within the high-speed supply channel exhibits swirling motions similar to the flow induced by a pair of counter-rotating vortices. The sense of rotation of the swirling fluid depends upon the orientation of the supply channel flow with respect to the crossflow, and in turn impacts the in-hole velocity fields. In the coflow supply channel geometry (channel flow is in the same direction as the free stream), a pair of vortices exists within the hole with the same sense of rotation as the primary jet counter-rotating vortex pair (CRVP). In contrast, the counterflow supply channel configuration has in-hole vortices of opposite rotational sense to that of the CRVP. The in-hole vortices interact constructively or destructively with the CRVP, thus affecting the strength and coherence of the CRVP. The counterflow configuration has a weakened CRVP because of destructive interference with the in-hole vortices. The weaker CRVP has a lower trajectory and increased spanwise spreading. External to the injection hole, a pair of vortices exists immediately downstream of the jet. They are initially perpendicular to the boundary-layer plate near the wall and are outboard of the streamwise hole centreline. These vortices, denoted ‘downstream spiral separation node’ (DSSN) vortices, are affected by both the supply channel feed direction and the blowing ratio. They appear to form by free-stream fluid wrapping around the jet and interacting with the CRVP. The coflow supply channel geometry is associated with the largest and most well-defined DSSN vortices, and their size is inversely proportional to the blowing ratio. At low blowing ratio, these vortices induce a large recirculating flow region downstream of the injection hole at the wall.

1. Introduction and objectives

During the past decade, there has been great interest in increasing the thrust-to-weight ratio of gas turbine engines. The impetus is for improving the performance envelope for military applications and for increasing energy efficiency for commercial aviation applications. Land-based turbines, used primarily for electrical power generation, will also benefit from enhanced performance. Demanding efficiency

requirements for modern gas turbines have driven the gas inlet temperature beyond the failure temperature of the turbine blade and vane material. To prevent failure in these hostile environments, rigorous cooling schemes are necessary. The primary technique for the cooling of gas turbine components is discrete-hole ‘film-cooling’, in which cooler air is drawn from the compressor and pumped through internal passages in the blade or vane and ejected through holes in the blade surface. The blade is cooled as the air passes through the inner passages and impinges upon the internal surfaces. The ejected air, being cooler and denser than the surrounding fluid, creates a thin protective boundary layer around the component.

Discrete-hole film-cooling configurations vary greatly depending on the application and whether the cooling scheme is being implemented on a blade or a stator vane. The jet-in-crossflow (JICF), which has been studied for many years, is the basic underlying canonical flow for film-cooling configurations. The jet/free-stream interaction produces a highly complex flow field that is dependent upon many geometric and hydrodynamic parameters. These parameters include, but are not limited to the blowing ratio ($M = \sqrt{\rho_j u_j^2 / \rho_\infty u_\infty^2}$), the length-to-diameter ratio of the holes (L/D), the spanwise hole spacing (P/D), the number of injection holes, the shape of the injection hole, the streamwise jet injection angle (α), the angle of the hole with respect to the free-stream (compound angle), supply channel geometry and flow direction, the temperature ratio of the crossflow and jet (related to the blowing ratio), and free-stream turbulence. These parameters affect such flow features as the jet trajectory, the induced pressure fields, the CRVP strength and coherence, the spreading angle of the jet in the spanwise direction, and in the case of film cooling, the surface heat transfer characteristics downstream of the injection holes (see LeBrocq, Launder & Priddin 1973; Colladay & Russell 1976; Hale 1999; Hale, Plesniak & Ramadhyani 1999a, 2000a,b; Hale, Ramadhyani & Plesniak 1999b; Yuan, Street & Ferziger 1999; Peterson & Plesniak 2002).

Despite many years of discrete-hole film-cooling and jet-in-crossflow research, there remain several unresolved issues, including the formation mechanism for the counter-rotating vortex pair (CRVP). Additionally, most previous work has focused on large hole length-to-diameter ratios (long holes). Film-cooling injection holes in next-generation gas turbine engines are expected to have L/D ratios close to unity (short holes). The hydrodynamics and heat transfer characteristics of short-injection-hole geometries have been studied much less than their large L/D counterparts. Examples of small L/D studies include those by Thole *et al.* (1996, 1997), Wittig *et al.* (1996), Burd & Simon (1998), Hale (1999), Hale *et al.* (1999a,b; 2000a,b), and Peterson & Plesniak (2002). In the following sections, conventional JICF results will be summarized followed by a discussion of the research issues and objectives associated with short hole JICF.

1.1. Features of conventional JICF

Jets in crossflow have been rigorously studied for several decades, as reviewed by Sherif & Pletcher (1990), Holdeman (1993) and Margason (1993). Past interest in JICF stemmed from such applications as pollutant distribution and V/STOL aircraft.

A jet issuing into a crossflow will bend in the streamwise direction. As the jet bends, fluid is entrained, and vorticity in both the issuing jet and the free stream stretches and aligns to form four dominant flow structures (see figure 1; adapted from

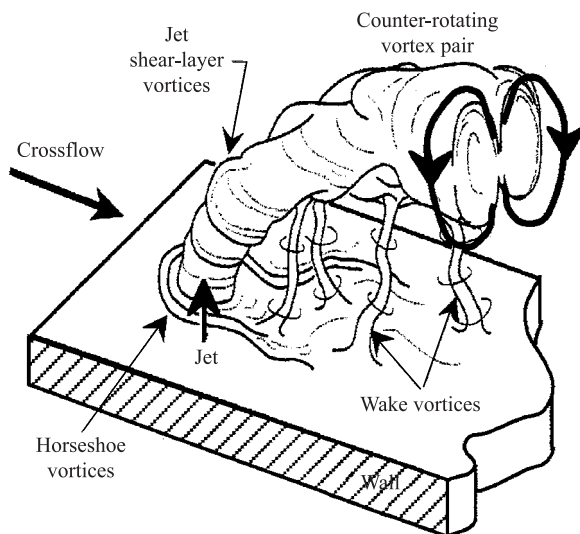


FIGURE 1. Structural features of jets in crossflow (adapted from Johnston & Khan 1997).

Johnston & Khan 1997). These four structures are:

(i) Ring vortices found on the upstream (windward) shear layer of the jet, produced by the Kelvin–Helmholtz instability in the shear layer.

(ii) A system of horseshoe vortices upstream of the jet, similar to those produced by a cylinder in a crossflow.

(iii) A pair of counter-rotating (kidney) vortices embedded in the jet.

(iv) A system of ‘wake’ vortices oriented in roughly the same direction as the original jet.

Studies of the shear-layer interaction have shown ring vortices on the windward side of the jet (see Becker & Massaro 1968; Fric & Roshko 1994), which are unsteady and become distorted as they progress downstream. The direction of rotation of the vortices is dictated by the vorticity in the jet shear layer. Kelso, Lim & Perry (1996) observed a steady ‘hovering vortex’, which wraps around the front and sides of the jet, that they suggest provides vorticity to the counter-rotating vortex pair. A large eddy simulation (LES) performed by Yuan *et al.* (1999) corroborated this observation.

Just upstream of the jet, horseshoe vortices form owing to the obstruction of the free stream by the jet and subsequent roll-up of the crossflow boundary layer. Many workers have stated that regardless of the genesis of the horseshoe vortices, they are weak and contribute very minimally to the structure of jets in crossflow (see Andreopoulos 1985; Kelso *et al.* 1996; Morton & Ibbetson 1996). Kelso & Smits (1995) and Yuan *et al.* (1999) observed the legs to either incorporate into the wake vortex structure or to be lifted away and merge with the CRVP, depending on the sign of the vorticity.

The dominant flow structure in JICF is the counter-rotating vortex pair. These vortices are created in the near field and occupy the entire jet cross-section, becoming synonymous with the jet in the far field. The length scales of these vortices are significantly greater than those of the eddies containing the turbulent energy and are therefore considered to be associated with the mean flow rather than the turbulence (see Morton & Ibbetson 1996).

One of the first attempts at explaining the CRVP formation was a two-dimensional potential flow analysis by Chang (1942), and subsequent reproduction by Margason (1969), of a deforming circular cylinder of fluid developing along the jet path with each time step. Though their analysis demonstrates the kinematics of the CRVP, it does not provide much insight into the formation mechanism of the CRVP. Morton & Ibbetson (1996) deduced that all deflected jets must contain the CRVP and that the pairs must form quickly. They also deduced that the CRVP progresses very far downstream because its vorticity is diffused very slowly. Hasselbrink & Mungal (2001*a, b*) presented detailed theoretical and experimental data on transverse jets at high blowing ratios. In part, they analysed the CRVP using the fundamental equations of motion in conjunction with scaling laws and found that an idealized vortex pair will have a constant angle of inclination throughout the entire jet, which is a function of the velocity ratio. Additionally, they discuss the circulation loss of the CRVP as the JICF progresses downstream and a method for predicting the length of the potential core.

The genesis of the counter-rotating vortex pair is still disputed and many hypotheses exist. Andreopoulos & Rodi (1984) proposed that for high velocity ratios (> 0.5) the CRVP vorticity is generated by the interfacial shear between the jet and the crossflow. However, vorticity cannot form anywhere within the interior of a homogeneous fluid (see Morton & Ibbetson 1996). Fric & Roshko (1989) contended that the CRVP is formed by the shear-layer vorticity of the jet. Kamotani & Greber (1972) and Foss (1980) suggested that the vortex pair is created in the wake behind the jet, while Crabb, Durao & Whitelaw (1981) claimed the CRVP can be visualized upstream of the injection hole and that the pressure gradient in the near hole region is responsible for forming the CRVP. Moussa, Trischka & Eskinazi (1977) suggested that the CRVP originates inside the hole by in-hole vorticity grouping into the vortices. Broadwell & Breidenthal (1984) likened the formation of the CRVP to the vortex formed by a wing and suggested that a 'lift' force impacted on the boundary layer by the penetrating jet formed the CRVP.

Morton & Ibbetson (1996) presented a very detailed description of a CRVP production mechanism, suggesting that the puncturing of the wall boundary layer by the jet creates the CRVP, whose azimuthal vorticity interacts with the boundary-layer vorticity and reorients, forming the two vortices. Yuan *et al.* (1999) proposed that the CRVP originates from quasi-steady vortices on each lateral edge of the jet. These vortices encounter an adverse pressure gradient as they approach the lee side of the jet and break down into the CRVP. Walters & Leylek (2000), in a computational study of streamwise injected jets, concluded that the two mechanisms that produce the CRVP are (i) the interaction of the jet with the free stream and (ii) the in-hole vorticity. They further concluded that the in-hole vorticity was the more significant of the two production mechanisms. Kelso *et al.* (1996) hypothesized that the roll-up of the jet shear layer is the mechanism that creates the CRVP, while Hale (1999) suggests that the CRVP is formed by the roll-up of boundary-layer fluid outboard of the jet and is intensified in the near jet region by the jet momentum.

Leylek & Zerkle (1994), simulating the experiments of Pietrzyk, Bogard & Crawford (1989), computed in-hole counter-rotating vortices of the same rotational sense as the primary CRVP in addition to the standard downstream vortex pair. Kohli & Thole (1997) performed calculations of a jet supplied by a plenum and were able to produce in-hole velocity fields containing either a pair of vortices or a single vortex. In both cases, the CRVP developed downstream of injection, implying that the CRVP is not simply the in-hole vortices advected into the free stream. Furthermore, Lemmon, Kohli & Thole (1999) determined from an Euler computation that a CRVP will form

downstream of an injection hole without any in-hole vorticity supplied and with slip along the surface (i.e. no boundary-layer vorticity). Caution should be exercised in interpreting inviscid numerical simulations because the effects of ‘numerical viscosity’ can lead to phenomena like those associated with physical viscosity.

A number of workers have discovered a second, much weaker and smaller pair of counter-rotating vortices, located under and having an opposite sense of rotation to the primary CRVP. Andreopoulos & Rodi (1984) were among the first groups to report the secondary CRVP, but did not suggest any definitive mechanism to explain its creation. Kelso *et al.* (1996) and Brizzi *et al.* (1997) reported similar observations experimentally, while Hale *et al.* (2000*a,b*) observed the vortices in their numerical simulations. Morton & Ibbetson state that the formation of the secondary pair is a direct result of their proposed CRVP formation mechanism.

Kuzo (1996) discovered a tertiary vortex pair while performing laser-induced fluorescence (LIF) and particle image velocimetry (PIV) measurements on a cross-section of a transverse jet at high velocity ratios (in the range $M = 5$, and, 25). Kuzo also discussed the asymmetry of the CRVP, stating that symmetry increases with increased Reynolds number. Smith & Mungal (1998), using planar laser induced fluorescence (PLIF), reported asymmetry of the scalar concentration field of the jets seeded with acetone vapour in the jet cross-section, under similar JICF parameters to those of Kuzo.

In some instances, the counter-rotating vortex pair has been reported to collapse into a single vortex. This is widely observed in compound injection angle cases, i.e. the jet is inclined not only to the flat plate, but also yawed with respect to the oncoming flow direction. This phenomenon was visualized by Broadwell & Breidenthal (1984) and numerically predicted by McGovern & Lylek (2000). Johnston, Mosier & Khan (2001), Khan & Johnston (2000) and Johnston & Khan (1997) describe such vortex-generating jets in detail.

Wake vortices are vertical structures observed downstream of the jet that join the CRVP and the wall boundary fluid. These structures were initially believed to be vortices shed from the jet, similar to the Kármán vortex-street observed in the wake of a cylinder (see Gordier 1959). As discussed by Fric & Roshko (1994), however, vorticity cannot be generated anywhere within the interior of a homogeneous fluid, and therefore the wake vortex formation mechanism cannot be the same as that which produces the periodic Kármán vortex-street. They further demonstrated that the wake vortices originate in the crossflow boundary layer, not in the jet.

1.2. Objectives

Results of an extensive experimental investigation of the velocity fields of the jet-in-crossflow emanating from short holes are reported herein. The particle image velocimetry (PIV) velocity fields are time-averaged to elucidate the mean flow structures. Statistical quantities such as the Reynolds stresses and r.m.s. velocities, as well as the mean vorticity are discussed qualitatively. The objectives are to explain the evolution of the jet velocity field starting from within the high-speed supply channel, through the injection hole, and out into the crossflow.†Furthermore, the formation and evolution of the counter-rotating vortex pair (CRVP) is discussed, as well as the effects of varying the blowing ratio and the supply channel feed direction.

† High-speed is used herein to connote that the velocity in the supply channel is of the same order as that through the holes, unlike that of a conventional plenum. It does not imply high Mach number flow.

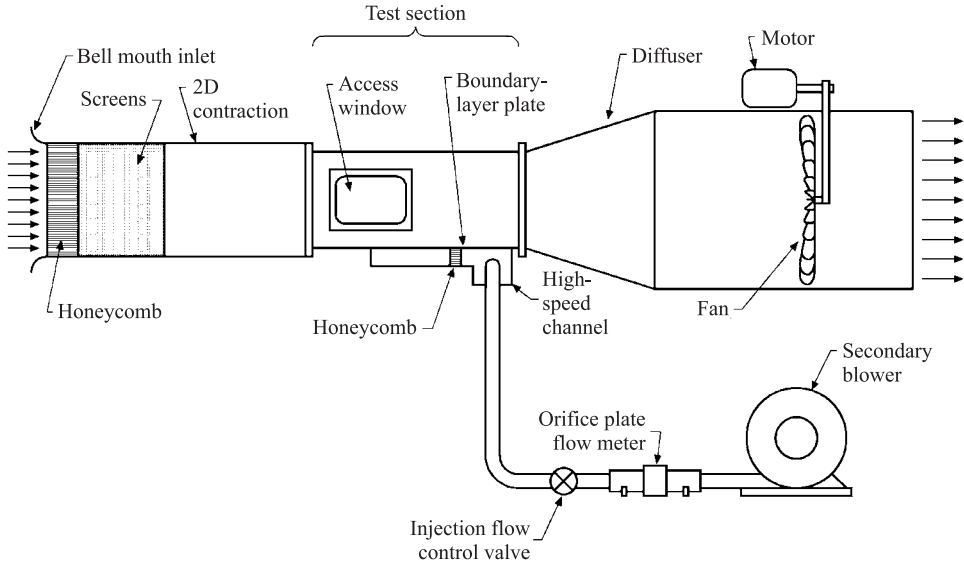


FIGURE 2. Low-speed wind tunnel and secondary flow loop schematic.

Finally, the role of in-channel and in-hole vortices and their implications for CRVP evolution are discussed.

2. Experimental methods

This section describes the experimental apparatus and PIV technique used to acquire the velocity fields.

2.1. Facility

A low-speed open-circuit wind tunnel was used in this investigation (see figure 2). The flow enters the tunnel through a rounded bell mouth inlet and proceeds through a flow-conditioning section consisting of a honeycomb section and four screens designed according to the recommendations of Loehrke & Nagib (1976) for suppression of free-stream turbulence. Following the flow conditioner is a 5:1 two-dimensional contraction with a fifth-degree polynomial contour design.

The optically-clear polycarbonate test section is 122 cm long with a 30 cm square cross-section. Downstream of the test section is a square-to-round diffuser to facilitate pressure recovery. The wind tunnel is capable of free-stream velocities between 2 and 30 m s^{-1} with turbulence intensities under 1%. The turbulence intensity was measured on a $25.4 \times 25.4 \text{ cm}^2$ grid of points in the free stream prior to the investigation using hot-wire anemometry to ensure uniformity and acceptable levels (Peterson 2001). Detailed information regarding the wind tunnel is presented in Wolochuck, Plesniak & Braun (1994, 1996).

A North American Mfg Co. T3D blower powers the secondary flow loop that provides the jet injection air. The jet flow enters the free stream via a high-speed supply channel designed to emulate the internal flow of a turbine inlet guide vane. Within the channel is a section of honeycomb to straighten the flow. The channel is sealed at the end, forcing all secondary air through the injection holes. The supply channel was designed to attach to the tunnel in either a coflow or counterflow configuration. Coflow denotes that the supply channel flow direction is the same as

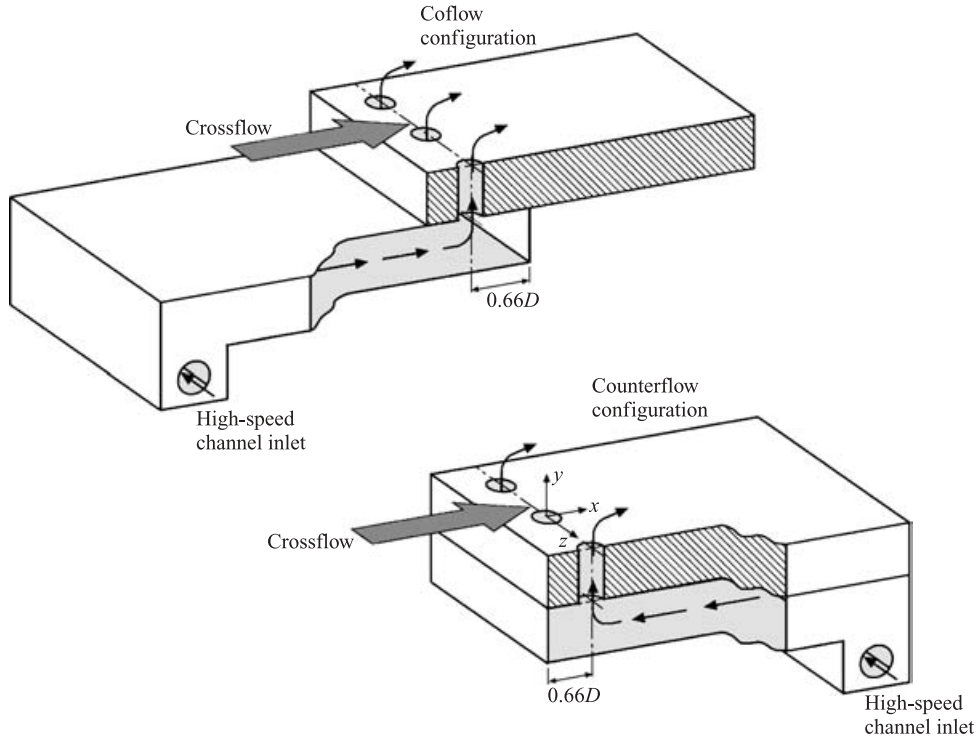


FIGURE 3. Supply channel flow configurations.

Hole diameter (D)	19 mm	Hole spanwise spacing (P/D)	3
Free-stream velocity (U_∞)	10 m s^{-1}	Endwall distance past hole (E/D)	0.66
Supply channel height (H/D)	1.0	Blowing Ratio (M)	0.5
			1.0
Hole length-to-diameter ratio (L/D)	0.66	Jet Reynolds number (Re_d) (based on M)	6000
B.L. thickness (δ/D)	0.83	B.L. Reynolds number (Re_δ)	10 500
B.L. momentum thickness (θ/D)	0.08	(Re_θ)	1024

TABLE 1. Experimental parameters.

the free stream, while counterflow denotes that the free stream and supply channel flow direction are at 180° to one another (see figure 3). The jet fluid issues into the crossflow from the wind tunnel floor via five spanwise-collinear injection holes. The injection holes are 19 mm in diameter, $0.66D$ long, and are spaced three diameters apart, a typical film-cooling configuration. Measurements are typically performed on the central hole. A summary of these and other relevant flow parameters is presented in table 1.

The boundary layer is ‘tripped’ upstream of the test section to create a turbulent boundary layer similar to that found in typical film-cooling applications. The trip-wire diameter and location were designed to achieve an effective Reynolds number (Re_x) at the hole location of 1.40×10^6 . For details regarding the boundary-layer trip, see Hale (1999). The boundary-layer velocity profile was determined to be fully turbulent using hot-wire anemometry (Peterson 2001). To further verify that the flow is turbulent, the

shape factor ($H = \delta^*/\theta$) was found to be 1.4, which is the typical value for a turbulent zero-pressure-gradient boundary layer.

2.2. Particle image velocimetry

Particle image velocimetry was used to determine the velocity distribution in multiple planes and orientations in the jet and the free stream. Data in the (X, Z)-plane (refer to figure 3 for coordinates) within the holes, and in the supply channel are presented as well.

2.2.1. Seeding

The jets and free stream were seeded with 1–3 μm diameter particles produced by burning a glycol-based fog fluid in a Rosco 1500 theatrical fog machine. Introducing theatrical fog directly into the secondary blower seeded the jet fluid, while free-stream seeding was accomplished by placing the fog machine near the wind-tunnel entrance and using the room as a plenum.

The works of Samimy & Lele (1991), Dring (1982) and Raffel, Willert & Kompenhans (1998) were used to confirm that the fog particles accurately follow the flow. Errors induced by tracer particles are primarily a result of gravity (sedimentation), particle inertia, and at small length scales, Brownian motion (which is not significant at the length scales of interest here).

Particle sedimentation velocity is determined by balancing the gravitational force and particle drag (see Raffel *et al.* 1998);

$$U_g = \frac{(\rho_p - \rho_f)d_p^2 g}{18\mu}, \quad (2.1)$$

where subscript p denotes particle properties, subscript f denotes fluid properties, and subscript g denotes settling due to gravity. This equation leads to a sedimentation velocity of 0.2 mm s^{-1} . The flow velocity scales are of the order of $1\text{--}10 \text{ m s}^{-1}$, or at least 1000 times greater, indicating that sedimentation effects are minimal.

Guidelines established by Dring (1982) and Samimy & Lele (1991) were used to ensure that particle inertia would not cause significant experimental uncertainty. The guidelines state that for optical techniques such as PIV and laser-Doppler velocimetry, the particle Stokes number, i.e. the ratio of the seed particle response time based on Stokes drag to the flow time scale ($St = \tau_p/\tau_f$) should be less than 0.2 for 2% maximum error in the velocity measurement. The particle response time based on Stokes drag, τ_p , is given by

$$\tau_p = \frac{\rho_p d_p^2}{18\mu}. \quad (2.2)$$

The flow time scale, τ_f , is given by

$$\tau_f = \frac{L_v}{U_v}, \quad (2.3)$$

where L_v is the eddy length scale and U_v is the eddy velocity scale. For a conservative estimate, the eddy length scale was chosen as the smallest length scale of interest (i.e. the smallest measured vortex diameter), and the eddy velocity scale was chosen to be 20% of the mean velocity, a typical value of eddy velocity in a shear layer. The ratio of the two time scales for the worst case combination of parameters in the current study is 0.04, therefore, it is expected that less than 2% bias error will be incurred due to particle inertia.

2.2.2. PIV hardware and analysis

The desired interrogation planes were illuminated by a New Wave 35 mJ/pulse Nd:YAG laser. The images were captured by a TSI PIVCam10-30 CCD array (1024 × 1024 pixels). The camera and laser were synchronized using a TSI Laser Pulse Synchronizer. Typical time intervals between images within a given pair were 20–40 μs with a delay of 0.272 ms between image pairs. One hundred image pairs were acquired for each experimental configuration, which after post-processing were temporally averaged using TecPlot software on a 600 MHz Pentium III personal computer. A hundred images were determined to be sufficient to provide convergence of the mean velocity data. This was determined by examining the in-hole mean velocity field based on averaging 5, 10, 20, 40, 60, 80 and 100 images. The mean fields for 60 and 80 time-averaged images were virtually identical, but 100 images were used to ensure convergence. To ensure no day-to-day variability in the experiments, data were collected and analysed for a few of the cases several times over a span of several days. These data showed no significant variation with respect to one another.

The vectors were validated using range, standard deviation, and median statistics. The TSI Insight 3.3 software package performed the cross-correlation using a typical fast Fourier transform method with a Gaussian peak-finding algorithm. A small number of vectors (typically less than 5%) were removed from each instantaneous measurement using range and standard deviation statistics. No interpolation or filling scheme was used to increase data density. The interrogation region was 32 × 32 pixels and was shifted 16 pixels (50% overlap) for each data point. The image size in physical dimensions varied from ~25 × 25 mm² for the in-hole data to ~90 × 90 mm² for the free-jet data. This yields a spatial resolution range from ~0.8 to 2.9 mm.

2.2.3. Uncertainty

The uncertainty in the PIV measurements is primarily due to locating the correlation peak in the cross-correlation field. Pixel displacement errors, based on the pixel resolution of the image, are estimated to be less than ±2.5%. Following the methods of Moffat (1998), combining pixel displacement errors with processing errors at a 95% confidence level yields uncertainty in the mean velocity measurements of ±3%. The uncertainty in the primary Reynolds shear stresses is estimated to be of the order of ±30%. This is a consequence of the limited ensemble size of 100 images to estimate statistical quantities. The ensemble size is a compromise between available data storage and processing capabilities and acceptable convergence of statistics. Statistical convergence for PIV data has been addressed by, for example, Uzol & Camci (2001) and Cater & Soria (2001).

3. Jet evolution

This section describes the detailed evolution of the flow from within the supply channel, through the injection hole, and into the crossflow for the 90°-injection hole with the counterflow supply channel at a blowing ratio of 0.5. Note that upstream and downstream, as well as leading and trailing edge, are defined with respect to the crossflow, which is always in the positive x -direction. Unless otherwise stated, the figures in this section will be oriented such that flow is from left to right, flood contours will indicate the local velocity magnitude, and streamtraces will illustrate the local flow direction.

3.1. Supply channel and in-hole hydrodynamics

3.1.1. Velocity field within the supply channel

Figure 4 shows the velocity field at various planes within the supply channel beneath the injection hole. The top measurement plane (P-5) is $0.05D$ below the jet hole entrance plane and each successive plane is $0.16D$ below the previous plane. Each measurement plane is less than $0.05D$ thick (1 mm).

In plane P-1, the flow approaches the hole from both the upstream and downstream direction, with the streams meeting along a 'line' approximately halfway between the hole streamwise centreline and trailing edge. Upon closer inspection, this 'line' contains critical points or singularities (points upon which all streamlines converge). As the measurement plane is traversed vertically, the 'line' in P-1 curls in on itself, forming a backwards 'C' in P-2 to P-3. Fluid near the endpoints of this line swirls with a rotation opposite to that of the primary CRVP of the jet. This can be observed with increasing clarity in planes P-2 to P-5. By planes P-4 and P-5, the in-plane fluid velocity near the hole circumference has increased as fluid is drawn into the injection hole. Note that in all of these measurement planes, the velocity magnitude of the fluid near the line containing the critical points is very low, while the fluid approaching this region is typically high. Therefore, it is likely that the low-velocity region distinguished by the aforementioned 'line' is where fluid is drawn strongly in the vertical direction (out-of-plane) towards the injection hole.

It has been postulated that in short-injection-hole geometries, the in-channel flow field significantly affects the jet characteristics because the flow cannot develop within the holes (see Hale 1999; Walters & Leylek 2000). In the current study, the observed in-channel flow structure appears to propagate through the hole and thus affect the crossflow.

3.1.2. In-hole velocity field

Figure 5 shows the in-hole velocity fields, which when viewed sequentially from the bottom of the hole to the top, illustrate the evolution of the in-hole flow structures. Owing to the large out-of-plane velocity component for this measurement, the time between PIV laser pulses is short ($23\ \mu\text{s}$). This is to ensure that the two pulses occur within the transit time of the seed particles through the 1 mm thick light sheet. The short time between pulses also decreases the in-plane distance that particles can move, thus increasing the uncertainty (if the distance travelled by the particles becomes small enough). However, since the primary goal is elucidation and comparison of flow structures, the potential increase in uncertainty of velocity magnitude does not impact the discussion significantly.

Plane H-1 is dominated by four mean vortical-like structures. The largest structures look qualitatively similar to stable spiral nodes from phase plane analysis of ordinary differential equations, while the smaller structures towards the trailing edge of the hole are ostensibly unstable spiral nodes (recall that flow towards a critical point is stable, while flow away from the point is unstable; Boyce & DiPrima 1997). Given the usefulness of the critical-point descriptors from phase plane analysis for describing these flow fields, they will be used throughout this section to describe and demarcate salient features. Additionally, throughout the remainder of the paper, a vortex within a PIV image shall be defined as a region consisting of circular (or near circular) streamlines. The sense of rotation of the larger stable spiral node vortices in plane H-1 is the same as the fluid within plane P-5 of the supply channel.

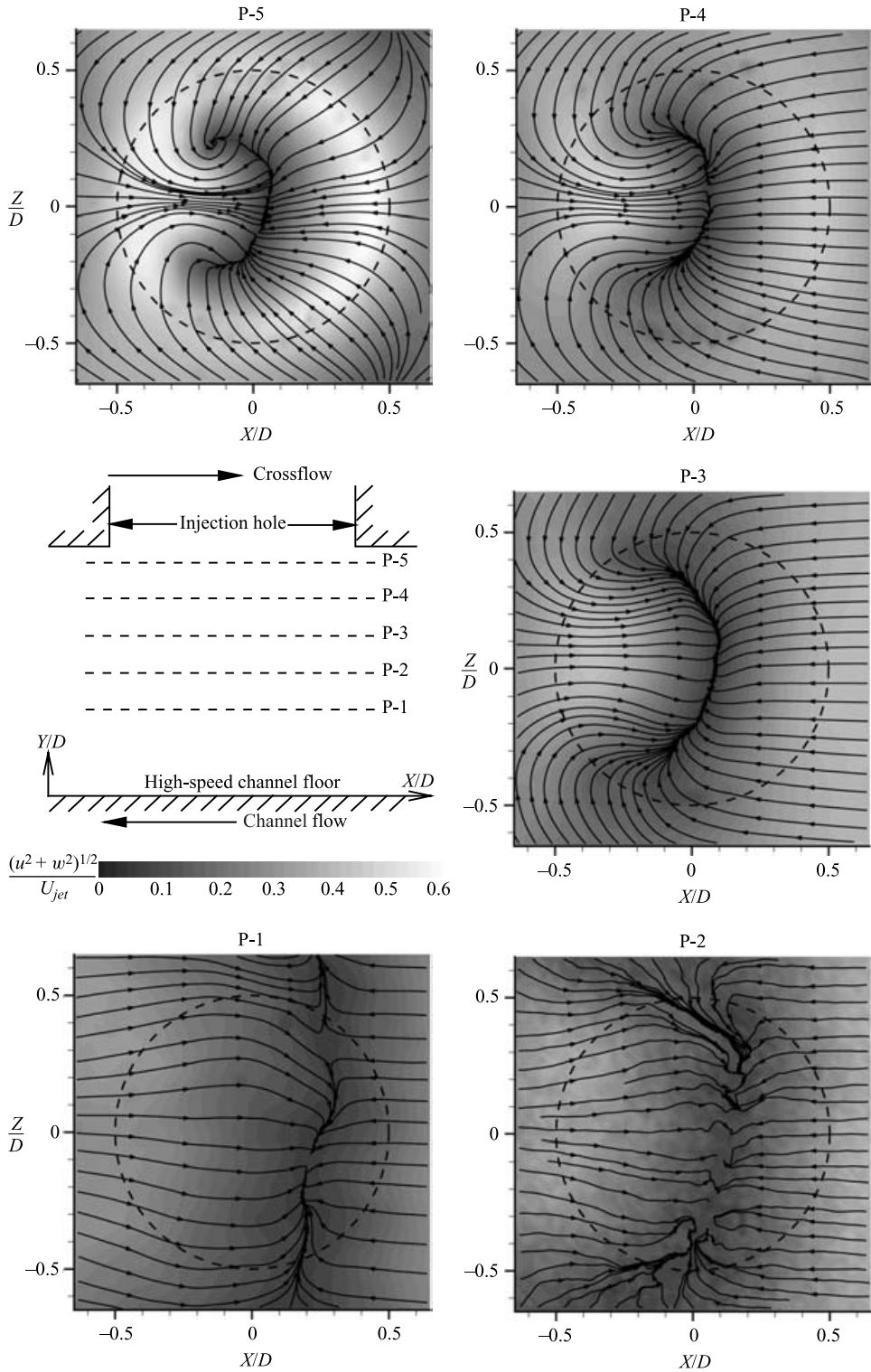


FIGURE 4. (X, Z) -plane velocity field within supply channel at various locations (90° short injection hole, counterflow channel, $M = 0.5$).

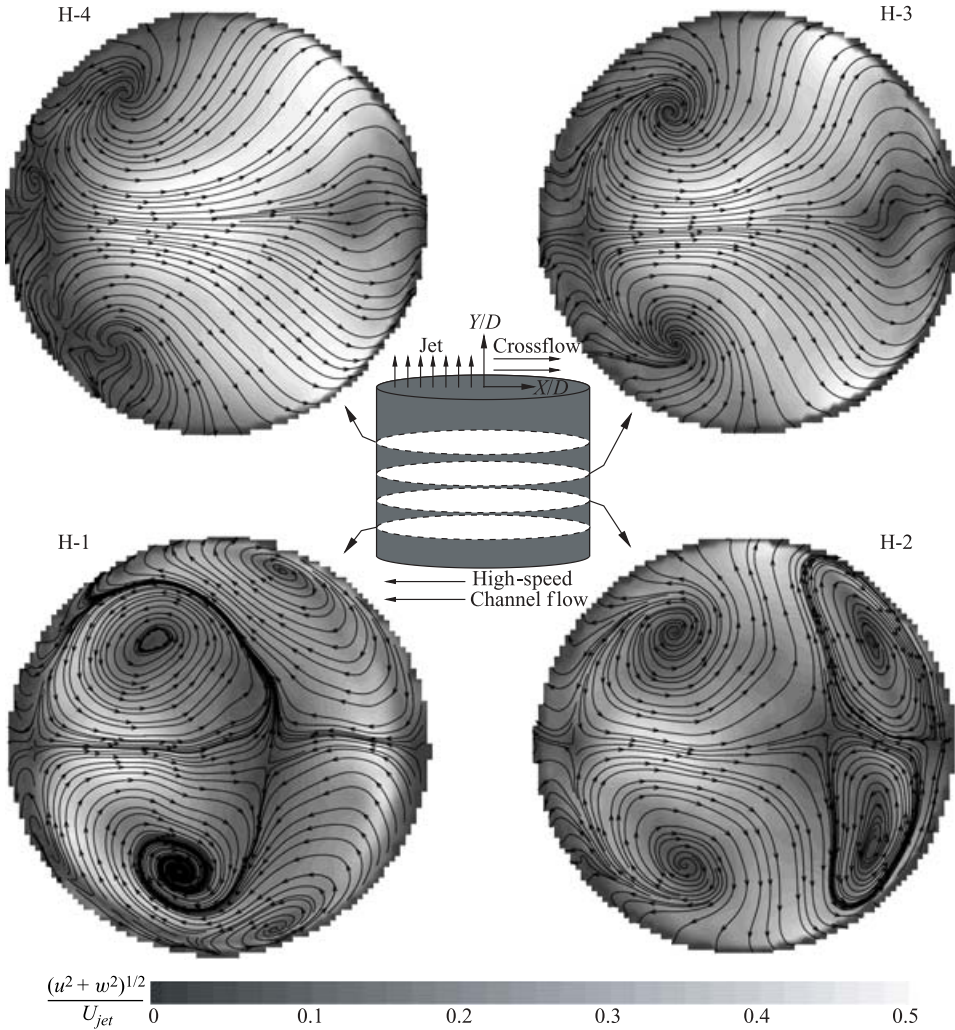


FIGURE 5. (X, Z) -plane velocity field within hole at various locations (90° short injection hole, counterflow channel, $M = 0.5$).

The two unstable spiral nodes are nearly mirror images of one another across the spanwise centreline. While the stable spiral nodes have the same sense of rotation as the in-channel fluid (opposite that of the jet CRVP), the smaller unstable spiral node vortices, while counter-rotating with respect to one another, have the same sense of rotation as the jet CRVP. The interaction of these four vortices in H-1 induces a saddle point along the spanwise centreline at $X/D = 0.12$. There is an additional saddle point near the leading edge of the hole, at $X/D = -0.43$. Recall that the leading edge is defined by the free-stream flow direction, not the channel flow direction. Flow between this second saddle point and the leading edge of the hole is in the opposite direction to the free stream. Flow is also in the negative X -direction between the first saddle point and the trailing edge of the hole.

Continuing to the second measurement plane, H-2, the large stable spiral node vortices of plane H-1 have become unstable spiral nodes, now radiating fluid from their respective cores, but rotating in the same direction as in H-1. They remain as

such for the remainder of the in-hole measurement planes. The large vortices have moved only slightly between the two measurement planes, while the two smaller vortices of plane H-1 (the original unstable spiral nodes) have migrated closer to one another and towards the trailing edge of the hole. The movement affects the location of the saddle point between the four vortices, moving it in the positive X -direction to $X/D=0.20$. In plane H-2, much of the bulk fluid motion is induced by the large in-hole counter-rotating vortex pair (IHCRVP), although the secondary vortex pair remains a salient feature. Migration of the smaller vortex pair alters the flow field, establishing a third stagnation or saddle point near the trailing edge, at $X/D=0.45$. While the reversed flow region near the smaller vortex pair has diminished by plane H-2, the reversed flow region near the leading edge has grown slightly, with the leading-edge stagnation point moving downstream slightly. This is consistent with the report by Brundage, Plesniak & Ramadhyani (1999) that the size of an in-hole separation region at the leading edge increases as the length of the hole is traversed.

Between planes H-2 and H-3, the smaller pair of vortices have apparently merged, annihilating one another. Diversion of the fluid towards the walls near the hole trailing edge is the only remnant of the original secondary vortex pair. The primary IHCRVP is still well defined, however, each vortex having moved in the negative X -direction approximately $0.05D$ since plane H-1. Hence, instead of four strong circulating regions as in plane H-2, there are now two circulating regions and a strong mean flow in the positive X -direction (free-stream direction). The saddle point near the leading edge is the only one that remains.

The velocity field at the final measurement plane, H-4, just before the fluid exits into the crossflow differs little from that in the third measurement plane. The primary vortices have pushed each other further towards the wall, and have moved slightly upstream. The residual flow field induced by the annihilated vortex pair is still observable, yet less apparent. Downstream of the vortices, the bulk fluid motion is in the streamwise direction, with a moderate divergence towards the outboard walls caused by the IHCRVP. The once clear leading-edge stagnation point is no longer visible, possibly because of the disrupting effects of free-stream ingestion. Free-stream ingestion is discussed by Brundage *et al.* (1999).

Note that in the previous and in future sections, discussion is primarily relegated to mean structures without reference to the instantaneous flow field. The instantaneous realizations for a number of cases have been analysed, however, and it appears that the dominant flow patterns are well represented by the average velocity field. The dominant vortices within the instantaneous flow fields are predominantly in the locations of the vortices within the mean field. There is undoubtedly some smearing by the spatial 'jitter' of the vortex locations. However, the existence of coherent structures in the average implies that the jitter is not severe.

3.1.3. Further discussion of in-hole vortices

In subsequent sections, it will be shown that in-hole vortices appear to significantly impact the CRVP, which is the dominant flow feature of the jet/crossflow interaction. In-hole vortices of the same rotational sense as the CRVP enhance the strength of the CRVP, causing a higher jet trajectory and decreased lateral spreading of the jet. This is an undesirable effect in applications such as film-cooling, where good coverage (jet remaining 'attached' to the surface) is essential for satisfactory operation. Conversely, in-hole vortices rotating in a sense opposite to the CRVP will diminish the CRVP and result in effects more desirable for film cooling.

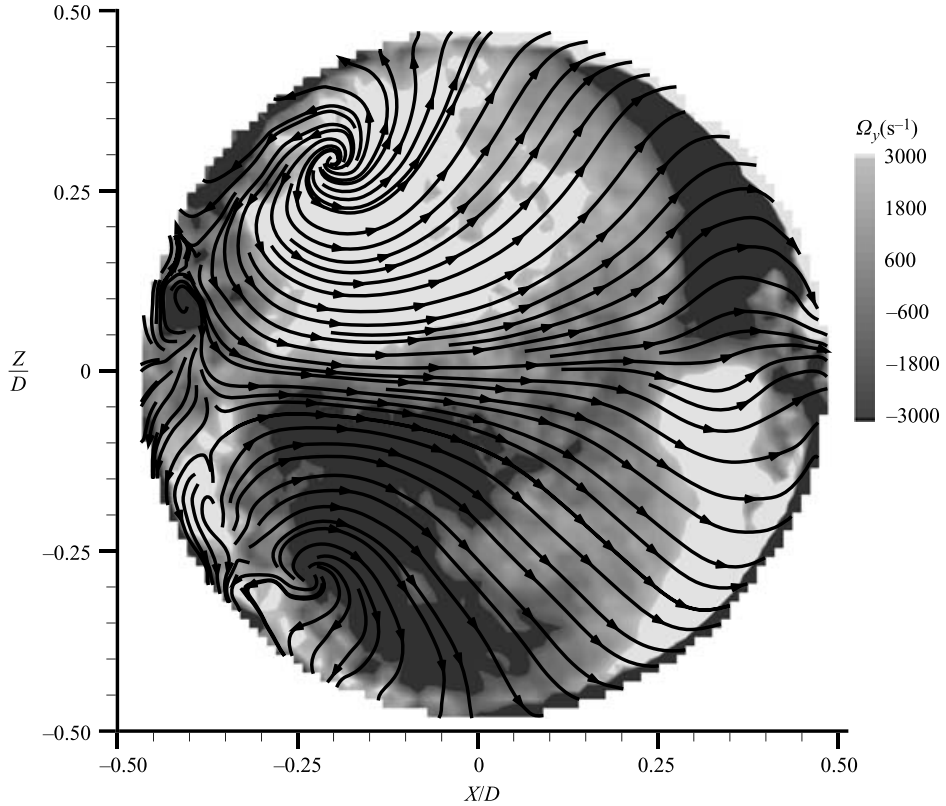


FIGURE 6. In-hole vorticity (Ω_y) $0.45D$ below jet exit plane (90° short injection hole, counterflow channel, $M = 0.5$).

Figure 6 shows the mean vorticity contours ($\Omega_y = (\partial u/\partial z - \partial w/\partial x)/2$) and vortical structures at plane H-4 within the injection hole. The vorticity was smoothed to eliminate small-scale disturbances, particularly near the injection hole wall. The purpose of this figure is to highlight rotation associated with the large-scale in-hole vortices, and not necessarily to provide quantitative vorticity magnitude. In this figure, the streamlines are overlaid by the mean vorticity contours. The light region corresponds to high positive vorticity, while dark flood contours indicate regions of high negative vorticity. Of course, vorticity can be used to identify vortical structures, although coherent vortical structures need not have vorticity, e.g. the case of a potential vortex (see Robinson 1991). In figure 6, the streamtraces assist in identifying the vortices, while the flood contours indicate the sense of rotation of the fluid.

Hale (1999) and Hale *et al.* (2000*a,b*) reported that the 90° short-injection-hole geometry with a counterflow supply channel at a blowing ratio of 0.5 produced anomalous hydrodynamic and heat transfer results when compared to other blowing ratios and supply channel configurations. This geometry was associated with decreased trajectory, increased spreading, and better film cooling performance. It was hypothesized that the CRVP for this geometry was much weaker. Figures 5 and 6 provide insight into why this configuration has the observed features. The in-hole vortices for this configuration are largely of opposite rotational sense to that of the CRVP in the jet. The in-hole vortex pair of opposite rotational sense is hypothesized to counteract and weaken the CRVP, thus causing the jet to remain very near the

wall and to spread more laterally. The strength and position of the CRVP will be discussed in §4.1.3.

3.2. Jet hydrodynamics

3.2.1. Mean spanwise jet velocity fields

Figure 7 shows the plan view velocity distributions of the jet efflux into the crossflow at various measurement planes parallel to the wind-tunnel floor. The first measurement plane, J-1, is located very near the boundary-layer plate. The laser sheet is skimming the surface, making the measurement height above the boundary-layer plate approximately the thickness of the laser sheet (~ 1 mm). Each subsequent plane is approximately 2 mm ($0.1D$) above the previous. Note that only the jets were seeded with tracers, so velocity data are available only where there is jet fluid.

Beginning at J-1, it is found that the velocity field over the injection hole is similar to that in the final in-hole plane, H-4. The fluid at the streamwise centreline of the hole is drawn outwards towards the jet boundary, similar to the in-hole fluid near the trailing edge. This is essentially an entrainment phenomenon, whereby the jet and free stream interact and exchange momentum. The most apparent difference between flow in plane H-4 and J-1 is that there are no vortical structures in the injection hole region of plane J-1. Whereas plane H-4 had the dominant in-hole vortical pair, no such vortices exist in plane J-1 over the injection hole. It appears that the dominant crossflow overpowers the vortices in the jet, thus washing them out. Superposing a vortex pair on a uniform free stream in a potential flow analysis illustrates this phenomenon (Peterson 2001).

Downstream of the injection hole, the jet/free-stream mixture accelerates and converges upon the spanwise centreline of the hole. Because the jet is not a bluff body, neither separation of the free stream from the jet nor vortex shedding can occur. Therefore, a true wake region does not develop behind the jet (see Fric & Roshko 1994; Morton & Ibbettson 1996). Rather, the CRVP draws fluid from regions outboard of the jet towards the jet centreline. As the centreline is approached, the action of the CRVP draws the fluid away from the wall, creating a region of low velocity downstream of the jet along the X -axis. Figure 8 shows the velocity field normal to the boundary-layer plate in the streamwise direction ((X, Y) -plane) along the hole centreline and demonstrates the lifting action of the CRVP (note the velocity outward from the wall in the region $X/D > 0.5$).

In addition to the lifting of the boundary-layer fluid downstream of the jet, a reversed flow region extends from the trailing edge of the hole to approximately $X/D = 1.65$. The end of this region is marked on figure 7(a) as ‘end of recirculation’. The reversed flow region, in conjunction with the flow induced by the CRVP, draws the outboard fluid in behind the jet, upstream, and into the jet.

Immediately downstream of the jet, two vortices roll-up. These vortices are both stable spiral nodes and are consistent with the time-averaged ‘wake’ vortices numerically predicted by Hale (1999) and Rudman (1996) and the whirlpools measured experimentally by Brizzi *et al.* (1997). Hale’s numerical prediction of these vortices is reproduced in figure 9 for a slightly different, yet comparable geometry and flow condition. Note that these structures are different from the wake vortex structures described by Fric & Roshko (1994), which are inherently unsteady and are formed by the roll-up of wall-boundary-layer fluid in a manner similar to the formation of tornadoes. Fric & Roshko did not study velocity ratios below two and found only weak wake vortices at the lowest velocity ratio. Rather, these vortices are associated with spiral nodes of separation (see Hale *et al.* 2000b). To distinguish them

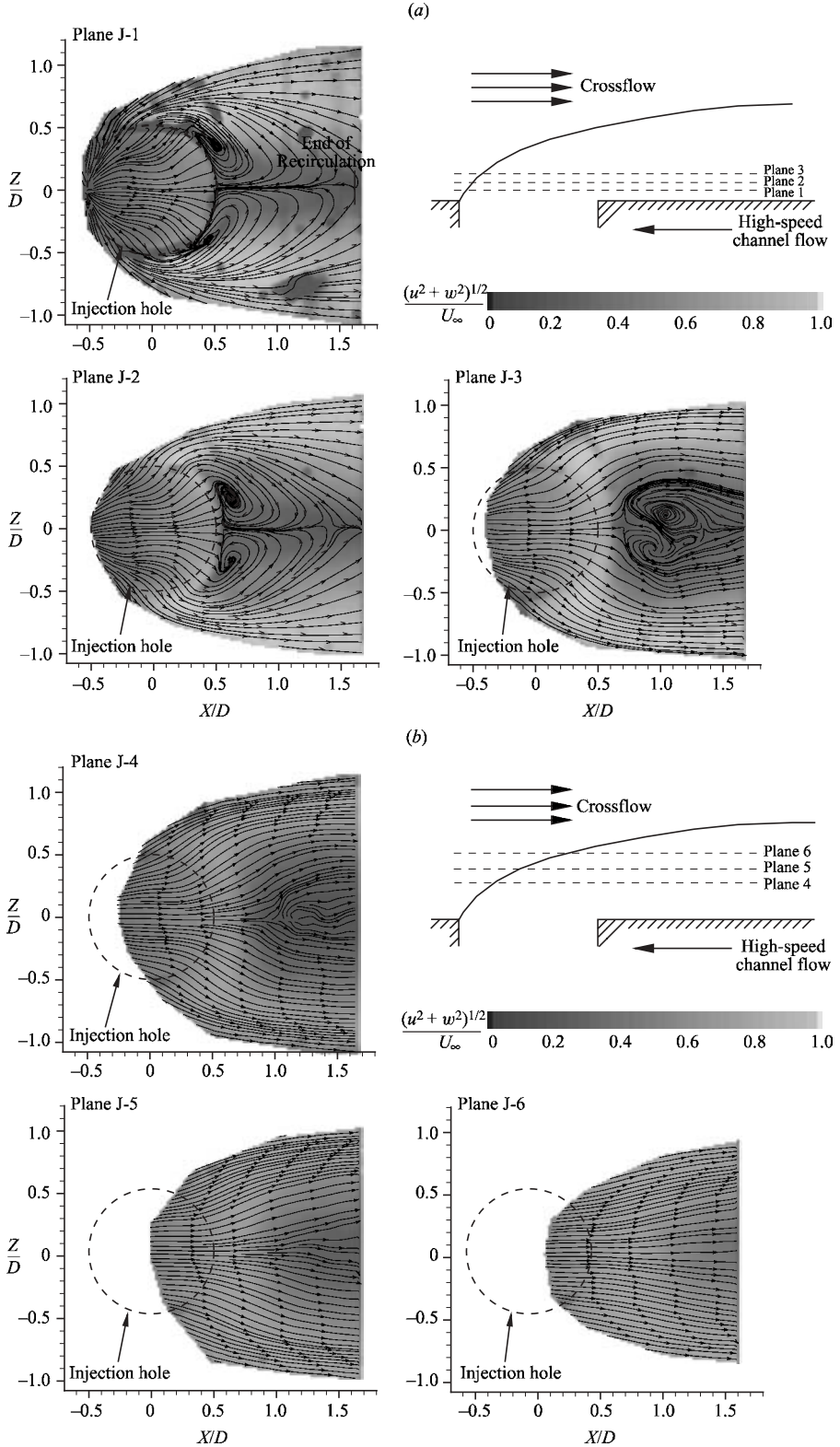


FIGURE 7. (X, Z) -plane velocity fields, (90° short injection hole, counterflow channel, $M = 0.5$). (a) Planes 1–3. (b) Planes 4–6.

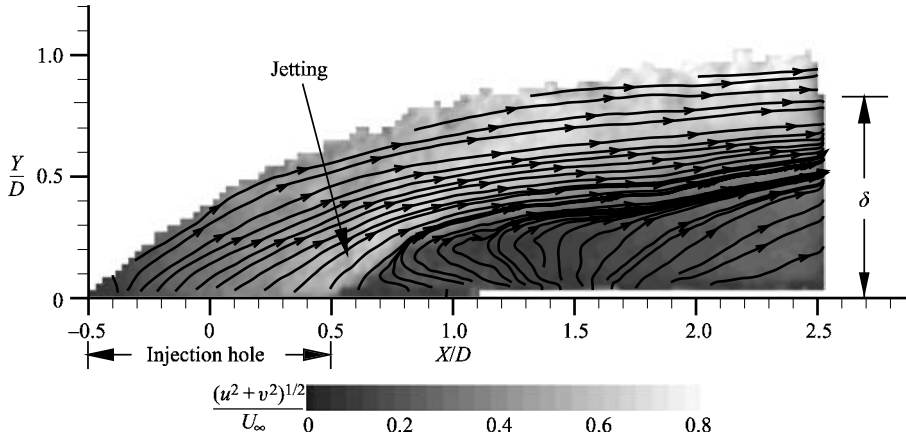


FIGURE 8. (X, Y) -plane velocity field at hole centreline (90° short injection hole, counterflow channel, $M = 0.5$).

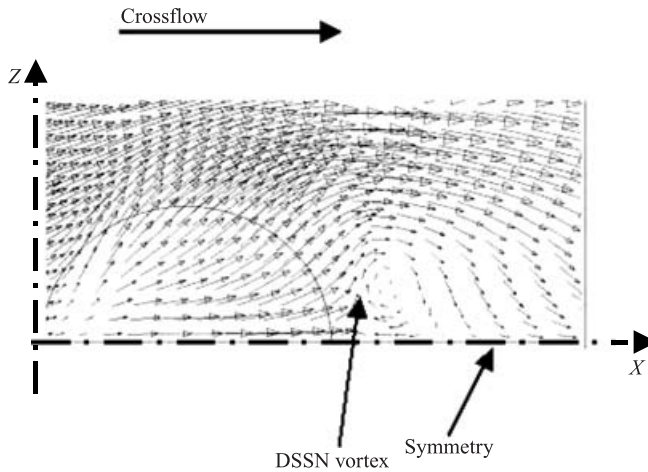


FIGURE 9. Numerically predicted DSSN vortex, $Y/D = 0.1$, $Z/D = 0$ (90° short injection hole, coflow channel, $M = 1.0$; from Hale 1999).

from the Fric & Roshko wake vortices, the steady ‘wake’ vortices will be referred to as downstream spiral separation node (DSSN) vortices for the remainder of this paper. Downstream of the DSSN vortices, fluid is still drawn strongly towards the jet centreline, where the velocities remain relatively low due to the action of the CRVP pulling fluid away from the wall.

Continuing away from the wall to planes J-2 and J-3 in figure 7(a), the DSSN vortices appear to have advected downstream and grown in size. It is not known whether the DSSN vortices actually grow as they move away from the wall, or if it is an illusion created by the projection onto the measurement planes of the vortices as they bend into the free-stream direction.

Still further from the wall, the contribution of the free stream (crossflow) to the in-plane velocity magnitude increases, owing to bending of the jet. Therefore, in-plane velocity is larger in magnitude in planes J-4 to J-6 than in the previous three planes. By J-4, the DSSN vortices observed in J-1 to J-3 are no longer distinguishable. Despite

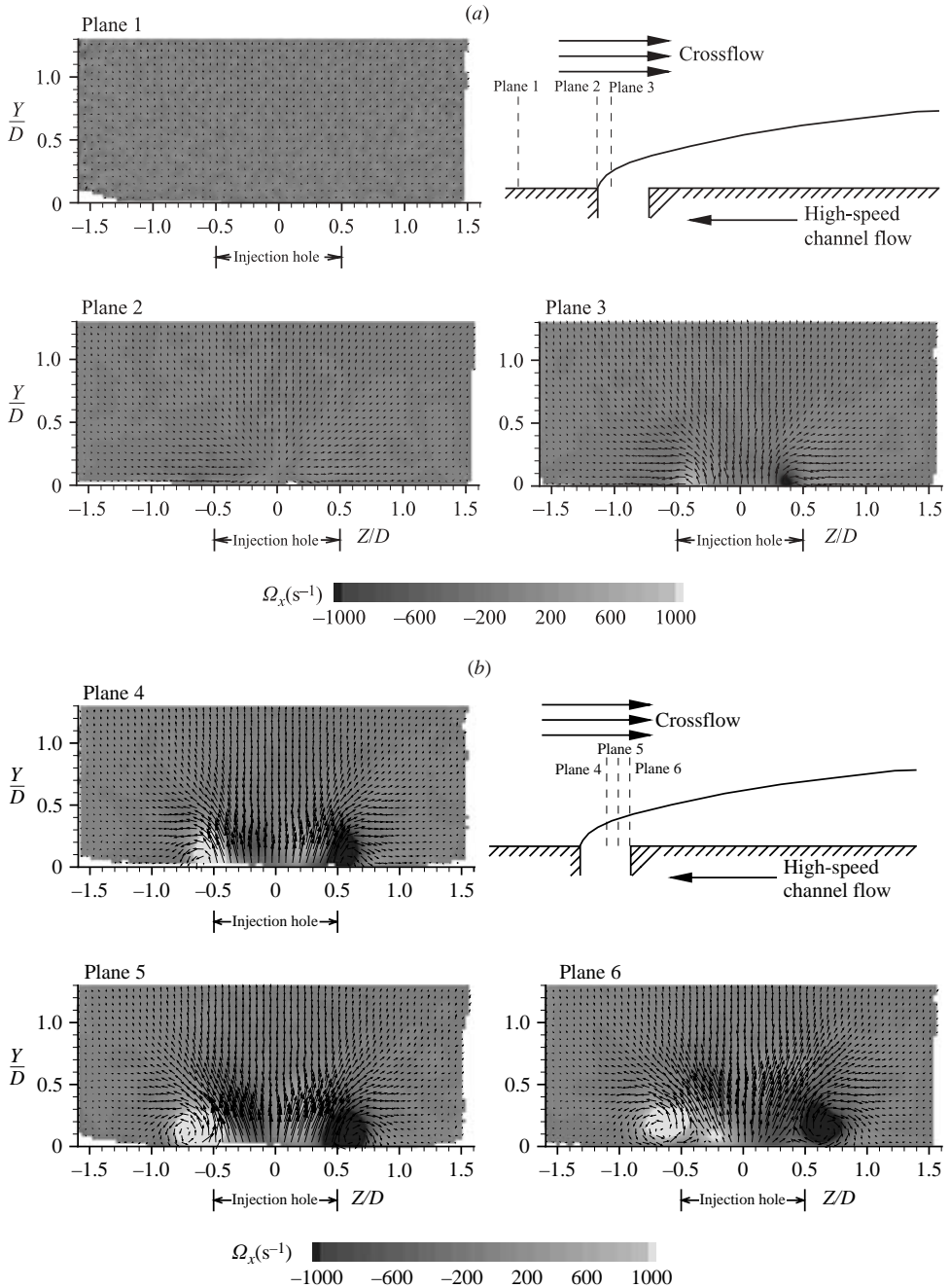


FIGURE 10(a, b). For caption see facing page.

the lack of coherent vortices, a low-velocity region within the jet continues to affect the remaining jet flow, which must accelerate around the region.

3.2.2. Jet cross-sectional velocity field and CRVP development

Figure 10 shows the velocity field in the (Y, Z) -plane (see figure 3 for spatial coordinate definitions) with overlaid mean streamwise vorticity contours of the

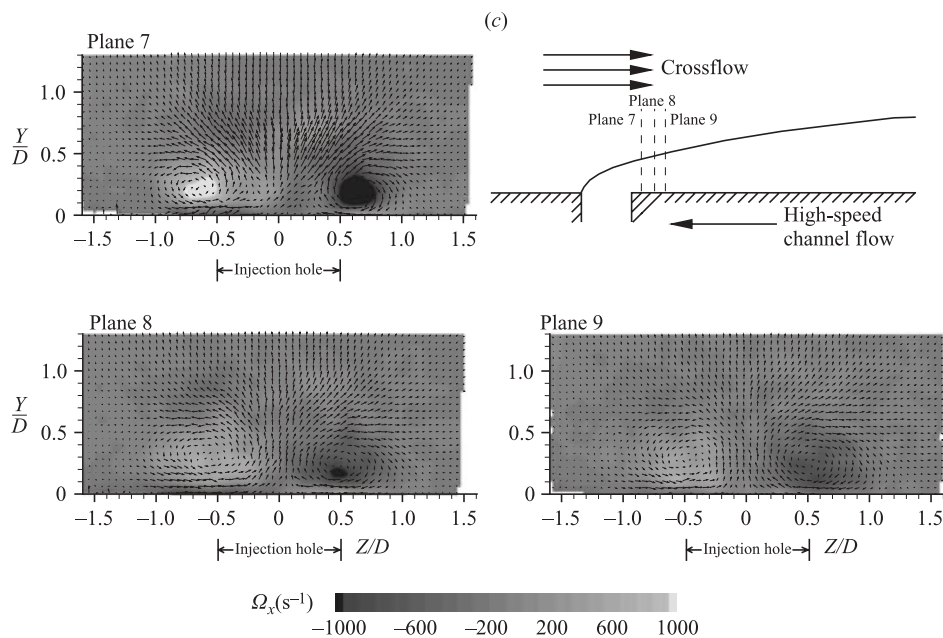


FIGURE 10. (Y, Z) -plane velocity and vorticity fields, (90° short injection holes, counterflow channel, $M = 1.0$). (a) Planes 1–3. (b) Planes 4–6. (c) Planes 7–9.

jet-in-crossflow at various X/D locations. To obtain these data, both the jet and free stream were seeded with flow tracers, thus making it impossible to differentiate between jet and free-stream fluid. A counterflow supply channel configuration at a blowing ratio of 1.0 is presented, instead of the 0.5 case presented previously. The trends are similar at $M = 0.5$, but they are easier to view at the higher blowing ratio because the jet is further from the wall and the counter-rotating vortices are stronger. All data will be made available as a supplement to the online version or from the *JFM* Editorial Office, Cambridge.

The streamwise locations of the planes beginning with plane 1 and progressing downstream are $X/D = -1.5, -0.5, -0.3, 0, 0.3, 0.5, 0.8, 1.2$ and 1.5. Plane 1, located $1.0D$ upstream of the hole leading edge, contains only boundary-layer fluid and is undisturbed by the upcoming jet. All of the cross-plane velocities in this plane are essentially zero. Recall that the dominant velocity component is out of plane for these figures (i.e. in the X -direction) with a magnitude of 10 m s^{-1} . The boundary-layer fluid begins to react to the upcoming jet disruption in plane 2, by moving radially outwards from the leading edge of the jet in association with a three-dimensional separation of the flow around the jet.

The strong vertical velocity component of the jet begins to shear the boundary-layer fluid outboard of the jet in plane 3, creating streamwise vorticity consistent with that of the CRVP. Shearing of the boundary-layer fluid is more pronounced in plane 4, corresponding to the streamwise jet centreline in figure 10(b) because the jet velocity increases towards the trailing edge of the hole owing to in-hole separations and higher velocity jetting. Thus, the high-vorticity regions at the hole edge are larger and small patches of streamwise vorticity appear to have advected out of the hole. These advected patches of vorticity are directly above the injection hole and are opposite in sign to the CRVP vorticity.

The velocity of the fluid exiting the hole near the centreline is slower than that at the edges of the hole. It is possible that this 'jetting' at the hole circumference is caused by a blockage of the flow by the in-hole vortices. In other words, the action of the in-hole vortices reduces the vertical velocity component of the fluid near the centre of hole, in the region of significant upstream flow. To compensate for the lower momentum of the fluid at the centre of the hole, the flow near the circumference must accelerate, producing the higher velocities outboard of the hole centreline.

The roll-up of the boundary-layer fluid into streamwise vortices at the edges of the jet continues in plane 5. Two vortical structures are present outboard of the jet and the jet velocity has increased (again, owing to trailing-edge jetting). Note that the centres of the vorticity contours do not correspond with the centres of the vortices. The vorticity presumed to have advected from the hole continues to move in the positive Y -direction. At the trailing edge of the jet, plane 6, the vortices induced by the shearing boundary fluid have moved away from the wall slightly. Additionally, a pocket of vorticity has appeared on each side of the hole centreline (near $Z/D = \pm 0.2$) with the same sign as the dominant vorticity on its respective side. Plane J-1 of figure 7(a) reveals that the locations and rotational sense of these vorticity patches correspond to those of the DSSN vortices discussed previously. It is conceivable that these vorticity patches are projections of the DSSN vortices in the (Y, Z) -plane.

Planes 7, 8 and 9 in figure 10(c) show the continuing development of the primary CRVP, which grows larger in scale and smaller in vorticity magnitude. The vortices migrate towards each other and away from the wall by mutual induction. Note that the vortices are asymmetric about the $Y/D = 0$ plane. The positive vortex is typically further from the wall, while the vorticity tends to be more concentrated for the negative vortex (this is not obvious from the figure, where the vorticity range is symmetric and with constant limits for comparison purposes).

It appears from these data in figure 10 that the CRVP forms by the shearing of the boundary-layer fluid by the jet. This qualitatively agrees with the hypothesis proposed by Hale (1999), which is in turn similar to the hypothesis of Yuan *et al.* (1999). Visual evidence also credits the vorticity interaction mechanism proposed by Morton & Ibbetson (1996). However, because it is not possible to differentiate between jet and free-stream fluid in these PIV results, it is not clear where the jet boundaries lie (particularly downstream of the jet), and thus it cannot be stated with certainty that the vortices form via these mechanisms. Another alternative is that the vortical structures outboard of the jet in planes 4–6 are the legs of the horseshoe vortex, and they merge with the CRVP downstream of the jet. Morton & Ibbetson (1996) reported, however, that the horseshoe vortices do not persist far downstream and that they are weak. By the time they pass the sides of the cylinder (jet) there is virtually no circulation remaining. To the contrary, the vortices discussed herein are not weak, nor are they lacking circulation (circulation will be discussed in a later section). Therefore, it is unlikely that these are remnants of the horseshoe vortices.

While these PIV data appear to support the boundary-layer shearing hypothesis for CRVP formation, other research groups have proposed many other notable formation mechanisms. Moussa *et al.* (1977) suggested that the CRVP originates within the hole by in-hole vorticity grouping into the vortices. The current study shows that while in-hole vortices impact the CRVP, the rotational sense of the in-hole vortices is not always the same as that of the jet CRVP. Additionally, Lemmon *et al.* (1999) reported that the shear layer between the jet and crossflow dictates the formation of the CRVP since a CRVP forms in the absence of boundary layers and in-hole vorticity in their inviscid numerical simulations. Crabb *et al.* (1981) claimed to observe the CRVP

upstream of the injection hole. In the current study, however, planes upstream of the injection hole indicate no vortical motion. Foss (1980) conjectured that the CRVP forms in the wake behind the jet. The (Y, Z) -plane PIV data indicate that the CRVP starts forming over the hole and influences the flow almost directly downstream of the injection hole.

The data did not reveal any secondary or tertiary counter-rotating vortex pair, e.g. as experimentally observed by Andreopoulos & Rodi (1984), Kelso *et al.* (1996), Kuzo (1996), Morton & Ibbetson (1996), Brizzi *et al.* (1997), and numerically predicted by Hale (1999). The secondary vortices are much smaller and weaker than the primary pair, making them more difficult to distinguish, particularly if they remain close to the wall. It is likely that the spatial resolution of the current PIV study was insufficient to detect structures with the predicted length scale of the secondary CRVP.

3.2.3. Jet cross-sectional Reynolds stresses and r.m.s. velocity

Figure 11 shows the Reynolds shear stresses $\overline{v'w'}$ in the (Y, Z) -plane in planes 4–9 (as defined in figure 10). The Reynolds stresses were obtained from 100 samples, which is insufficient for statistical stationarity. However, these data are presented for their qualitative insight, as opposed to quantitative value. The upstream planes have been omitted because they contain no significant Reynolds stresses.

In general, the Reynolds shear stress is concentrated around, but not centred on, the counter-rotating vortices. A second region of elevated shear stress exists above each vortex and is of opposite sign (e.g. see plane 7 in figure 11*b*). This distribution shows that the turbulence is not only concentrated around the CRVP, but also exists above the CRVP. Regions of high turbulence production are associated with the shear layers created by the jet and crossflow interaction and CRVP velocity field. To further illustrate the regions of high turbulence, the r.m.s. velocity $[\overline{v'^2 + w'^2}]^{1/2}$ (in planes 4–9) is presented in figure 12. In the planes over the injection hole (planes 4–6 in figure 12*a*), the highest r.m.s. velocity is located near the shear-layer interaction outboard of the jet (in the location of the forming CRVP). As with vorticity and Reynolds shear stress, the position of highest r.m.s. velocity is not coincident with the centres of the forming vortex pair. As the CRVP proceeds downstream, both the Reynolds shear stress and r.m.s. velocity concentrations spread out, indicating that the turbulence is diffusing across the jet cross-section as the jet develops downstream.

4. Blowing ratio and supply channel direction effects

The effects of changing the supply channel feed direction (refer to figure 3 for supply channel orientations) and blowing ratio are discussed next. Of these parameters, the supply channel feed direction was found to have the most significant impact on the flow fields.

4.1. Effects of supply channel feed direction

4.1.1. In-channel flow field

The supply channel feed direction has a profound effect on the in-channel flow field. Thole *et al.* (1996, 1997), Wittig *et al.* (1996), Walters & Leylek (2000), Burd & Simon (1998), and Hale *et al.* (1999*a,b*, 2000*a,b*) reported a strong dependence of the external flow field on the supply channel feed direction for short injection holes. They based their conclusions upon numerical simulations, velocity measurements and flow visualization. Figure 13 shows the velocity field at the measurement plane nearest the jet entrance (plane P-5) within the supply channel for the two supply

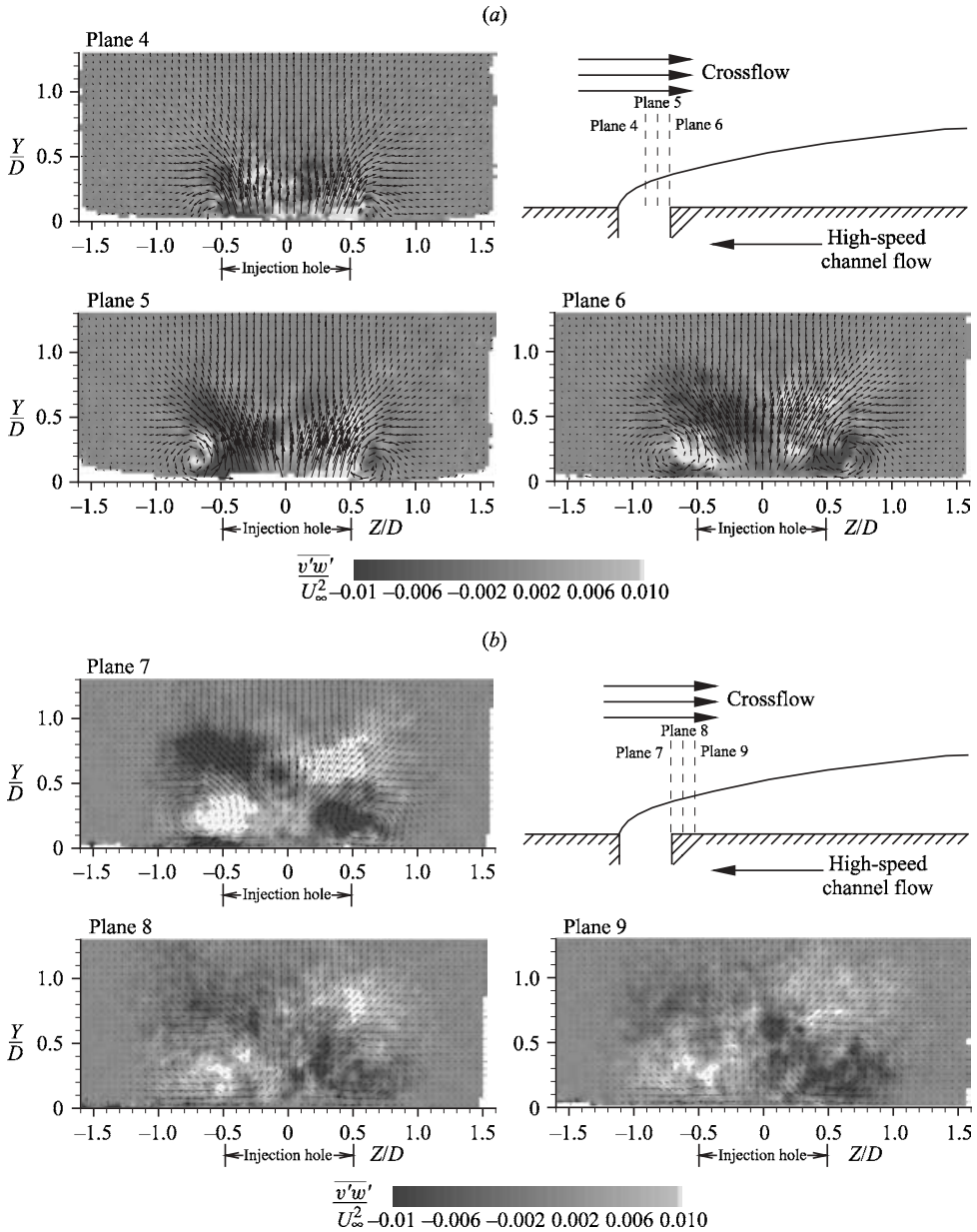


FIGURE 11. (Y, Z) -plane Reynolds stress fields, (90°) short injection holes, counterflow channel, $M = 1.0$. (a) Planes 4–6. (b) Planes 7–9.

channel configurations at a blowing ratio of 0.5. Reversing the supply channel feed direction alters the rotational sense of the in-channel vortices. The coflow supply channel has in-channel vortices of the same rotational sense as the primary jet CRVP (clockwise), whereas the counterflow supply channel generates counter-rotating vortices of opposite rotational sense to the CRVP (counterclockwise). The consequence of this is that the jet associated with the coflow supply channel geometry has a higher trajectory and less lateral spreading than that for the counterflow geometry (see

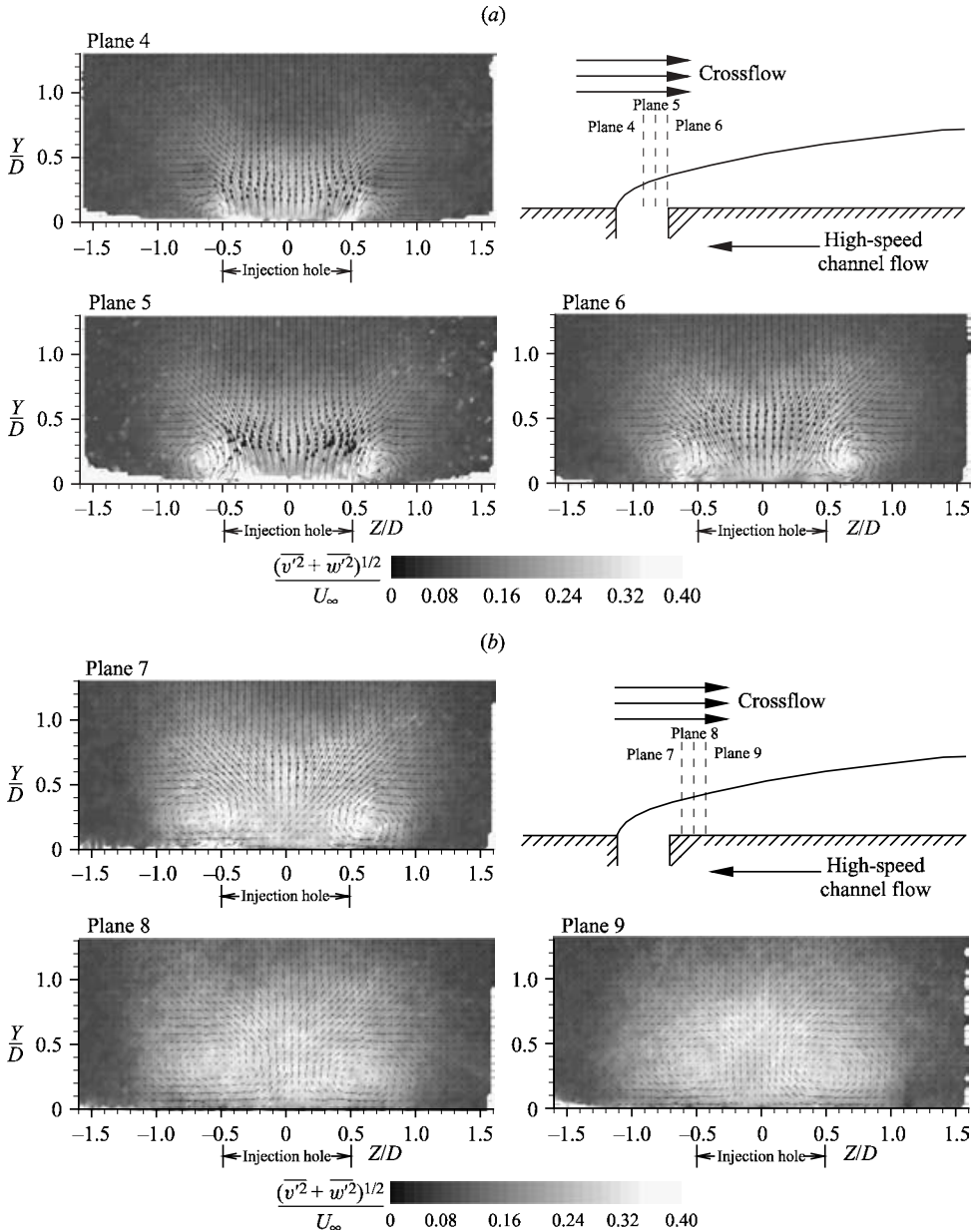


FIGURE 12. (Y, Z) -plane r.m.s. velocity fields, 90° short injection holes, counterflow channel, $M = 1.0$. (a) Planes 4–6. (b) Planes 7–9.

§4.1.3). This is, in part, due to the enhancement of the CRVP by in-channel and in-hole vortices.

4.1.2. In-hole flow field

For the coflow supply channel geometry, the in-hole vortices are biased towards the trailing edge of the injection hole, and rotate in the same direction as the jet CRVP. A comparison of the in-hole velocity field with overlaid vorticity contours for each supply channel flow configuration at the plane nearest the jet exit (H-4) is

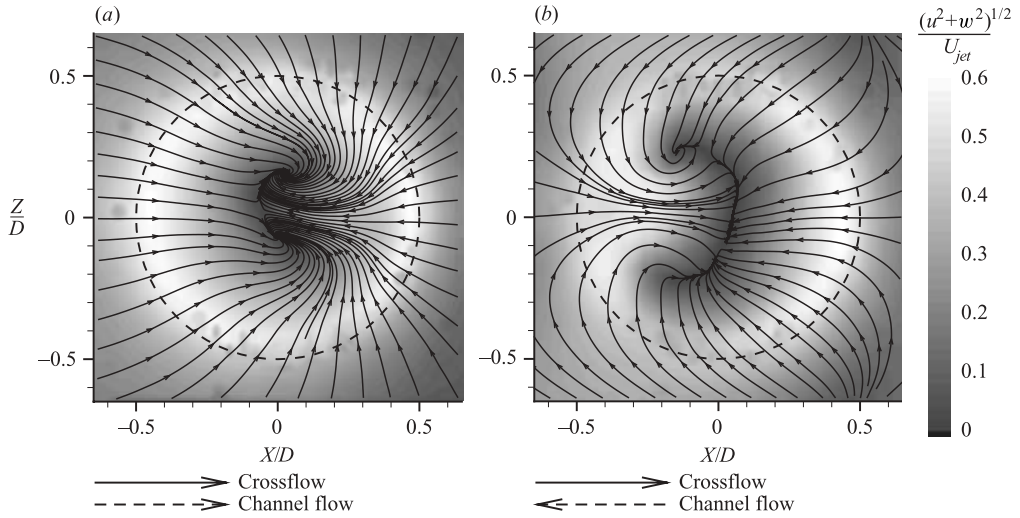


FIGURE 13. Comparison of in-channel flow fields at $M = 0.5$, plane P-5 (a) coflow channel, (b) counterflow channel.

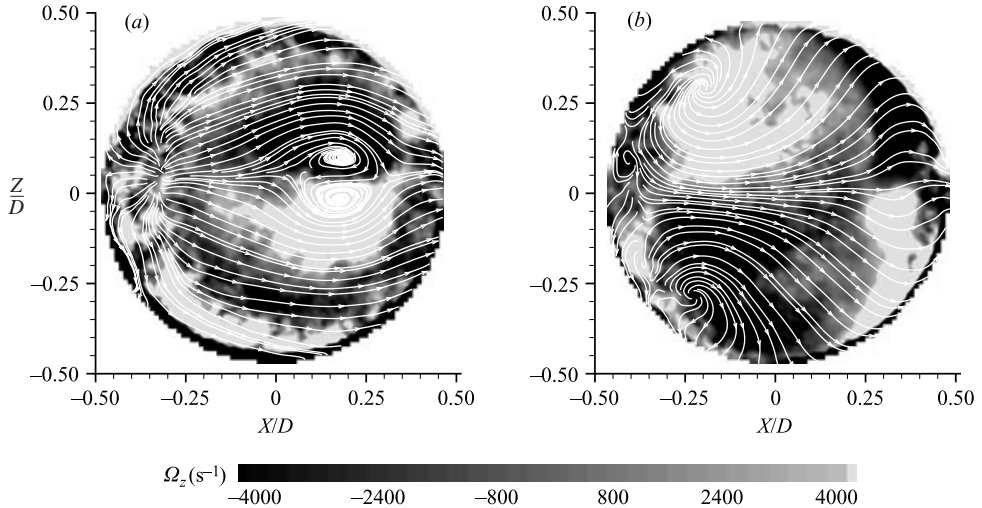


FIGURE 14. Comparison of in-hole structures and vorticity at $M = 0.5$, plane H-4 (a) co-flow channel, (b) counterflow channel.

shown in figure 14. The in-hole flow structures are affected by the location of in-hole separations of the fluid as it moves from the supply channel to the free stream. In the coflow supply channel, the in-hole separation occurs at the leading edge of the injection hole, whereas the counterflow supply channel has a separation at the trailing edge.

In the coflow configuration, because the free stream and the supply channel flow are oriented in the same direction, redirection of the flow is minimal. The separation on the hole leading edge is severe, however, which induces a circumferential velocity component and causes the formation of a vortical structure near the trailing edge of the hole. The counterflow supply channel, on the other hand, has a separated region at the trailing edge of the hole. In this orientation, the free stream and the supply

channel flow direction are 180° to one another; hence, the flow must make a sharp turn to enter the free stream. This causes a strong reversed flow within the hole that impinges upon the leading-edge wall and jets circumferentially around the hole perimeter.

4.1.3. Jet flow field

As mentioned previously, the supply channel feed direction affects both the trajectory and the spreading of the jet. In general, the coflow supply channel JICF has a higher trajectory and less spreading than the counterflow supply channel JICF. This is shown in figures 15 and 16, which are the comparisons of the two supply channel configurations in the (X, Z) and (X, Y) -planes, respectively.

The difference in spanwise spreading angles is subtle in figure 15 because the velocity data were truncated near the jet boundary, but the angle of the streamlines with respect to the streamwise direction is indeed greater for the counterflow configuration. Other workers have previously reported the decreased spreading of the coflow supply channel (see Hale 1999). In terms of the near-hole flow structures, the trajectory and spreading affect the DSSN vortices and the low-velocity region within the jet, downstream of the injection hole. The DSSN vortices in figure 15 are smaller in the counterflow supply channel geometry. In this configuration, the jet fluid does not converge as rapidly upon the spanwise centreline downstream of the hole. This leaves a larger region of velocity deficit in the downstream jet and weaker DSSN vortices. The strength of these vortices appears to be dependent upon the strength of the CRVP, i.e. weaker DSSN vortices are associated with a weaker CRVP.

Figure 16 compares the (X, Y) -plane velocity fields for the co- and counterflow supply channel geometries. The fluid exiting the injection hole for the coflow case has a much stronger vertical velocity component than for the counterflow case, which causes a higher trajectory. This is also consistent with a stronger CRVP. There appears to be a separation point in the low-velocity region downstream of the jet. Streamlines emanate from a location roughly 1.3 hole diameters downstream of the hole centreline in both cases. The region that the streamlines emanate from is apparently larger for the counterflow case. However, the jet remains closer to the wall in this case, thus making this assessment difficult; particularly, since data near the wall typically has a greater uncertainty.

4.2. Effects of blowing ratio

4.2.1. In-channel and in-hole flow fields

Within the supply channel, varying the blowing ratio from 0.5 to 1.0 did not influence the types of flow structure that were observed. The magnitude of the velocity within the supply channel increased, but the overall flow features remained approximately the same. However, the blowing ratio did have significant impact on the in-hole flow features. Whereas for low blowing ratios in the counterflow supply channel configuration the flow field is very symmetric, a high degree of asymmetry exists at higher blowing ratios (see figure 17). The fluid generally flows in the upstream direction for the blowing ratio of 1.0 case because of the separation at the trailing edge of the injection hole and the momentum of the jet fluid. Upon entering the injection hole, the fluid impacts the leading edge of the injection hole and diverts circumferentially around the hole perimeter. At the higher blowing ratio, there is essentially one dominant vortex in the injection hole. This is similar to the in-hole structure numerically predicted by Kohli & Thole (1997) for a perpendicular crossflow fed by a standard plenum.

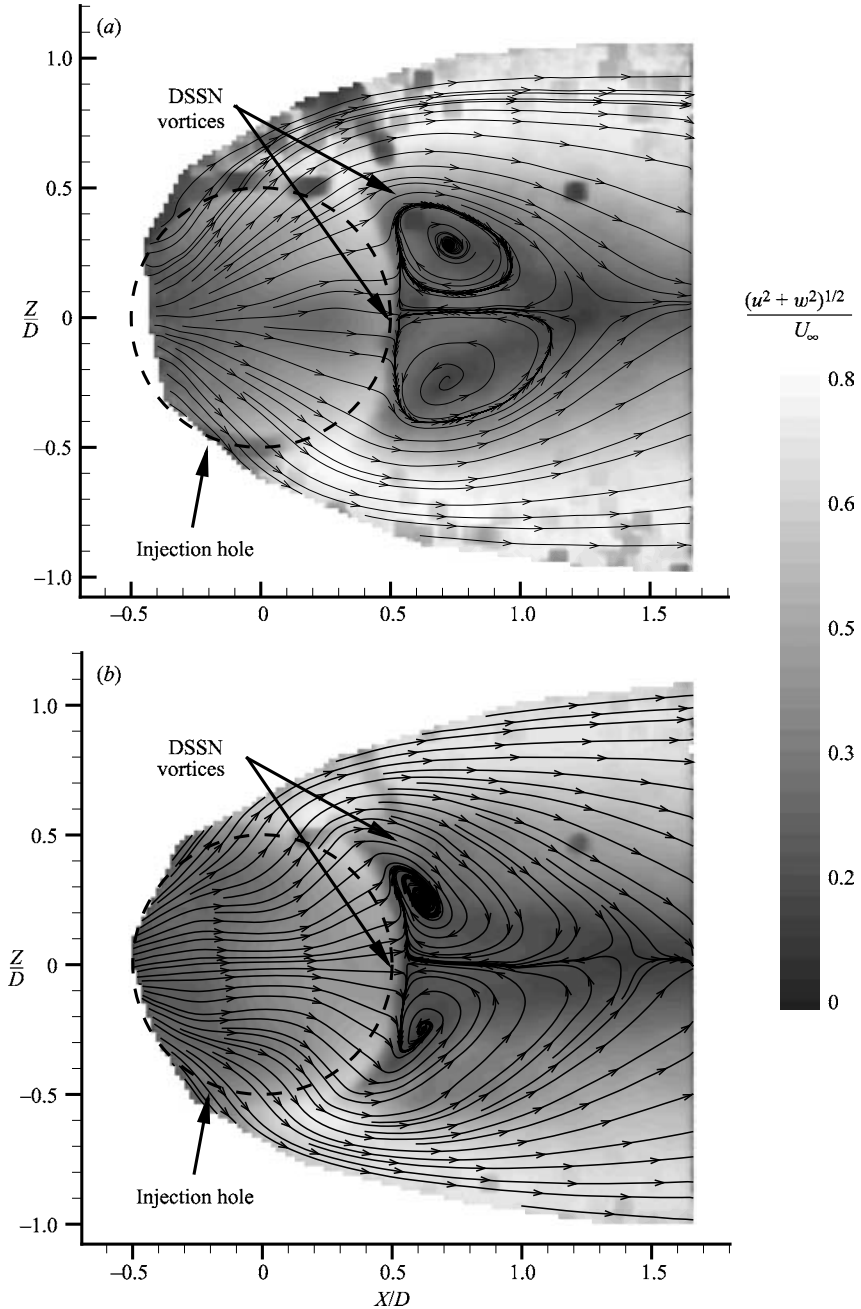


FIGURE 15. Comparison of (X, Z) -plane velocity fields at $M=0.5$, $Y/D=0.13$ (a) coflow channel, (b) counterflow channel.

Asymmetries in JICF are not uncommon. Kuzo (1996) and Smith & Mungal (1998) reported asymmetries in the CRVP of the JICF for velocity ratios between 5 and 25. Both reported that nominally symmetric flows develop asymmetries for various flow configurations. Kuzo reported a Reynolds-number dependence and created a regime map, whereas Smith & Mungal found no Reynolds-number dependence. They

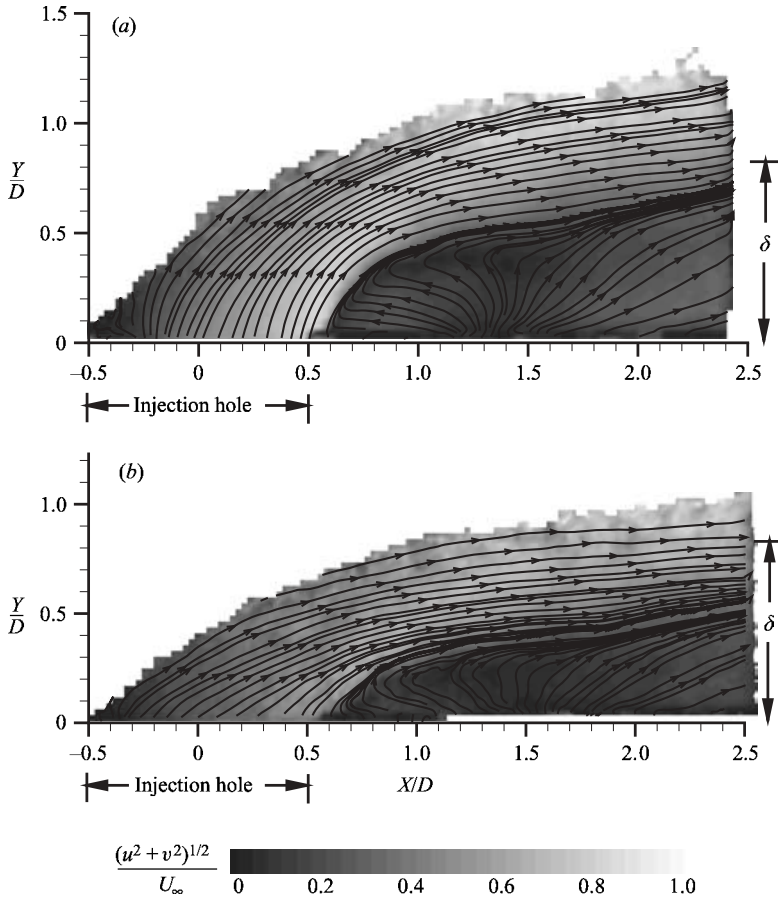


FIGURE 16. Comparison of (X, Y) -plane velocity fields at $M = 0.5$, centreline plane (a) coflow channel, (b) counterflow channel.

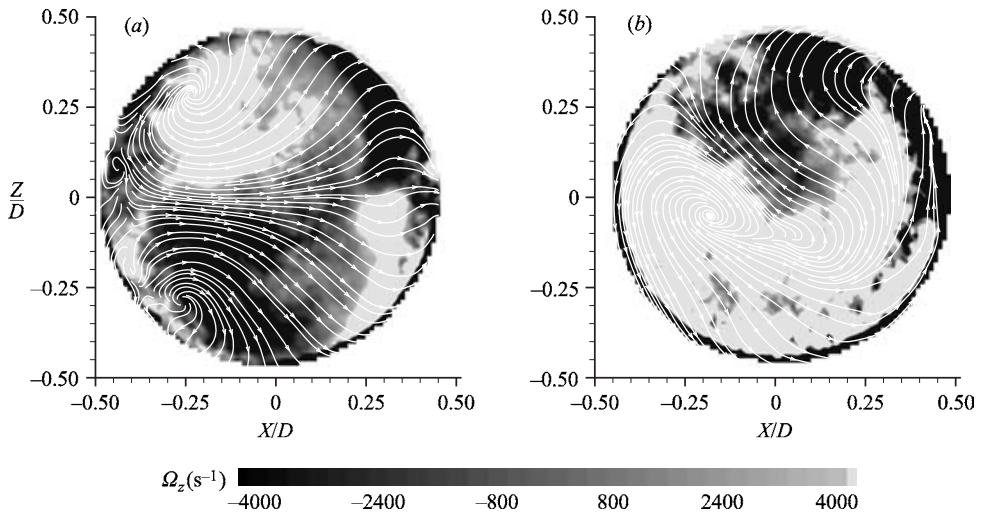


FIGURE 17. Comparison of in-hole vorticity for counterflow channel, $Y/D = 0.45$ (a) $M = 0.5$, (b) $M = 1.0$.

were unable to find a dependence on any flow parameter and were unable to predict when asymmetry would occur from any JICF theory. In the current study, the in-hole velocity field was measured several times during different runs and the asymmetry persisted. It is a repeatable phenomenon that appears to be a function of the blowing ratio, with the lower blowing ratio producing a more symmetric velocity field. This is consistent with the report of Kuzo (1996) that the higher blowing ratios were more asymmetric. Cusano & Plesniak (1999) reported asymmetries in the CRVP in a rectangular JICF with velocity ratios ranging from 0.5 to 1.5. In all of these studies, the cause(s) of these asymmetries is still unknown.

4.2.2. Jet flow field

The most prominent effect of the blowing ratio is on the strength of the DSSN vortices and the length of the recirculation zone immediately downstream of the injection hole in the measurement plane immediately above the wall (J-1). A comparison between the $M=0.5$ and 1.0 cases is shown in figure 18. For higher blowing ratios, the DSSN vortices are poorly defined and cover a relatively small area of the jet cross-section, as shown in figure 18(b). At lower blowing ratios, however, the DSSN vortices are more coherent structures, spanning a large region of the downstream jet (figure 18a). A possible explanation for this is that for the higher blowing ratio, the CRVP is stronger and draws the relatively weak DSSN vortices into its structure earlier in the jet development. Another possibility is that the steady DSSN vortices are inherently weaker at large blowing ratios and thus have a much weaker induced flow field and smaller recirculation region. Note that this behaviour is quite different from that of the Fric & Roshko (1994) ‘wake’ vortices, which are stronger at higher velocity ratios.

Perhaps the most surprising effect of blowing ratio concerns the length of the recirculation zone. For blowing ratios of one, the length of the recirculating zone is decreased by as much as half a hole diameter, or over 33% compared to that for the blowing ratio of 0.5. The length of the reversed-flow region is a function of the pressure field induced by the jet on the wall. At high blowing ratios, the jet lifts from the wall rapidly, so the fluid is rapidly drawn into the jet from the boundary layer. This effect is shown in the (X, Y) -plane velocity field comparison for the two blowing ratios in figure 19. Over this range of blowing ratios, the wall pressure gradient is influenced more strongly by the distance of the CRVP from the wall than the circulation (strength) of the vortices; see Peterson (2001). For high blowing ratios, the jet has a higher trajectory and lifts from the wall very near the jet exit hole. Therefore, the effect of the jet upon the boundary-layer fluid does not persist as far downstream as in the case of low blowing ratios, owing to the proximity of the jet to the wall. At low blowing ratios, the jet remains near the wall for a greater distance downstream and therefore affects the boundary-layer fluid over a greater distance.

4.3. Comparison of CRVP location

Figure 20 shows the wall-normal cross-sectional velocity field at $X/D=1.5$ for the four cases considered. The location of the CRVP centre is marked for each case. The centre was determined visually by examining the velocity field data. Comparing the co- and counterflow cases, it is apparent that for the counterflow cases, the CRVP centres are further apart and that they are closer to the wall. This is consistent with the trajectory and spreading angle data reported by Hale (1999). Comparing the $M=0.5$ and $M=1.0$ cases, it is observed that decreasing the blowing ratio decreases the trajectory and the lateral spreading. Again these effects are consistent

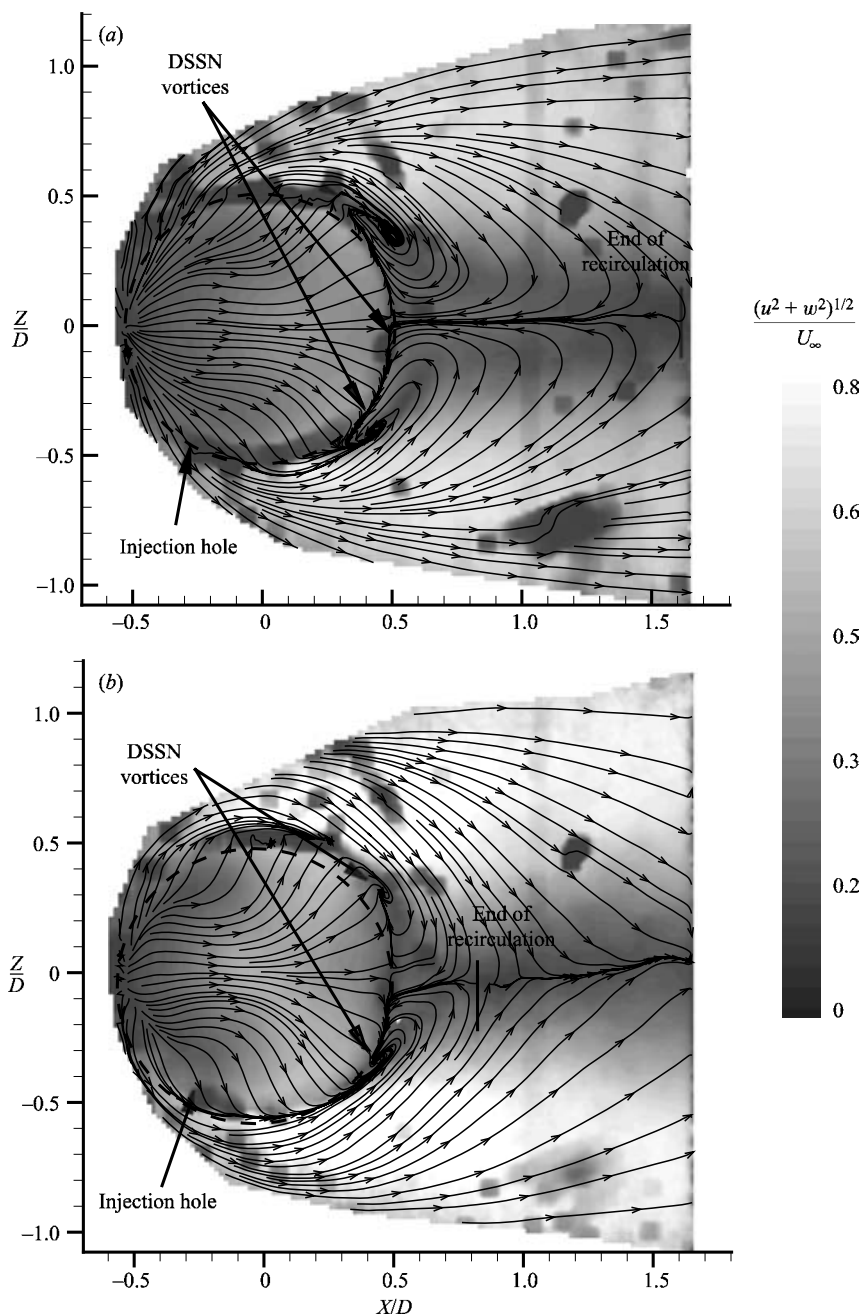


FIGURE 18. Comparison of (X, Z) -plane velocity for counterflow channel, plane J-1
(a) $M = 0.5$, (b) $M = 1.0$.

with expectations based on the relative strength of the CRVP in these cases. The circulation of each vortex in figure 20 was calculated by performing the line integral around an isovorticity contour and is reported in table 2. The contour level used for each calculation is presented in table 2. The circulation shows that the coflow channel has a stronger vortex pair than the counterflow channel at the same blowing ratio.

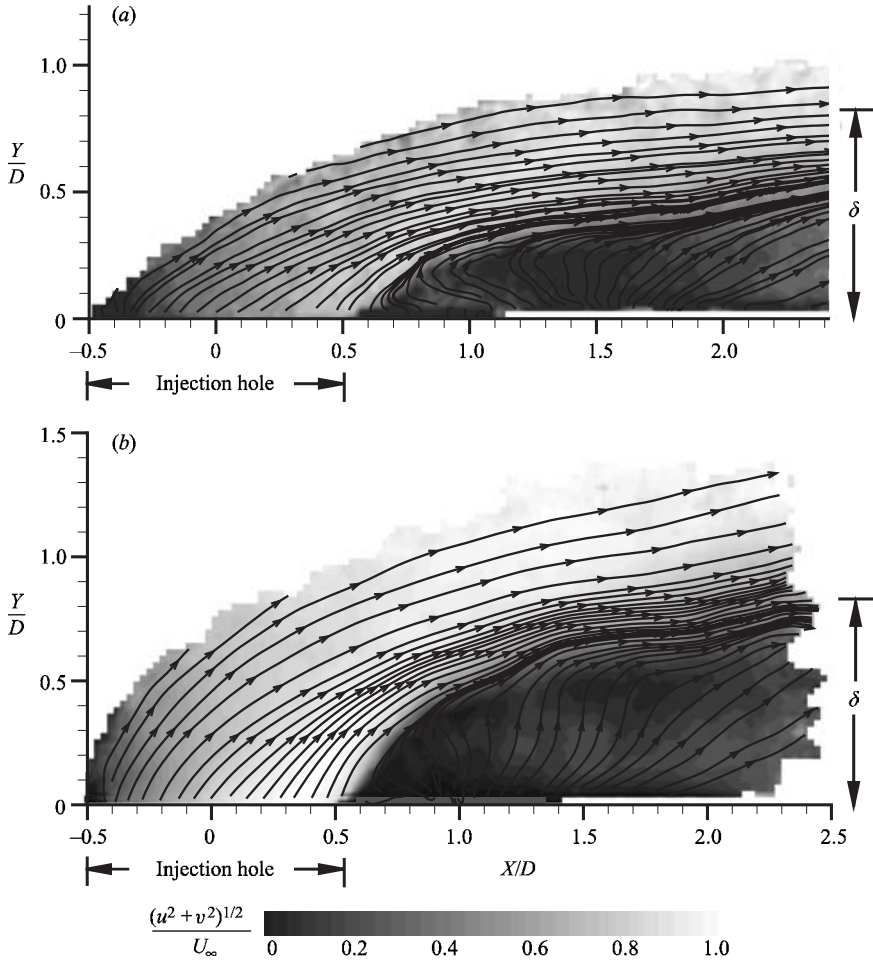


FIGURE 19. Comparison of (X, Y) -plane velocity for counterflow channel, centreline plane
(a) $M = 0.5$, (b) $M = 1.0$.

	Γ/UD
Coflow, $M = 1.0$ ($\Omega = \pm 2800 \text{ s}^{-1}$)	
Left	-0.472
Right	0.460
Coflow, $M = 0.5$ ($\Omega = \pm 500 \text{ s}^{-1}$)	
Left	-0.083
Right	0.141
Counterflow, $M = 1.0$ ($\Omega = \pm 500 \text{ s}^{-1}$)	
Left	-0.172
Right	0.123
Counterflow, $M = 0.5$ ($\Omega = \pm 500 \text{ s}^{-1}$)	
Left	-0.050
Right	0.033

TABLE 2. CRVP strength for various configurations.

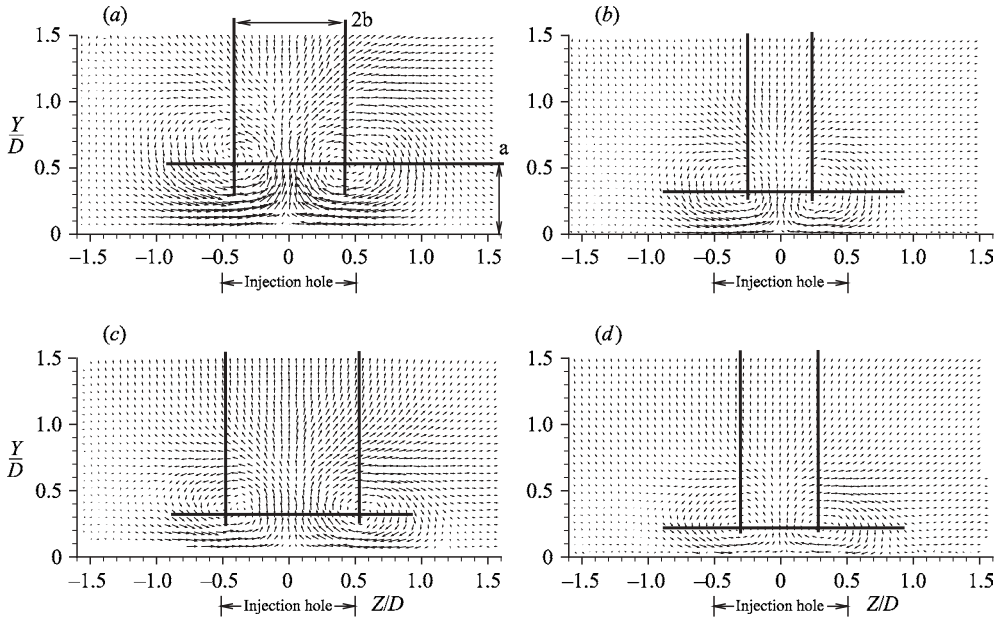


FIGURE 20. (Y, Z) -plane velocity fields and CRVP locations. (a) coflow, $M = 1.0$; (b) coflow, $M = 0.5$; (c) counterflow, $M = 1.0$; (d) counterflow, $M = 0.5$. $X/D = 1.5$.

Additionally, a blowing ratio of unity produces a stronger vortex pair than a blowing ratio of 0.5.

5. Conclusions

The velocity field evolution of a short hole ($L/D < 1$) jet-in-crossflow from within the supply channel, through the hole and into the crossflow was studied using PIV. Furthermore, the blowing ratio and the supply channel feed direction were varied over a range of interest in gas turbine cooling applications. Both parameters were found to affect such flow features as the trajectory of the jet, the lateral spreading of the jet, and the low-velocity region downstream of the jet. Blowing ratio in the range of $M = 0.5$ to $M = 1.0$ was found to significantly affect the trajectory and the spanwise spreading of the jets. As the blowing ratio was increased, the trajectory and spanwise spreading both increased. Though it is desirable from a film-cooling perspective to increase the spanwise spreading, thus increasing the coverage, the benefit is overshadowed by the increased trajectory and ‘lifting’ of the jet from the wall, allowing hot gases to penetrate to the wall. The higher blowing ratio ($M = 1.0$) was associated with reduced size of both the DSSN vortices and the recirculation zone downstream of the injection holes compared to the $M = 0.5$ case.

Perhaps counterintuitively, increasing the blowing ratio from 0.5 to 1.0 reduced the streamwise extent of the backflow region downstream of the injection holes by up to 33%. At high blowing ratios, the jet moves away from the boundary-layer plate quickly. The high-velocity fluid of the jet entrains boundary-layer fluid near the wall downstream of the jet. However, the distance downstream that the jet affects the near-wall fluid is relatively short. For lower blowing ratios, the jet issues from the hole and remains much closer to the wall, and the vortices within the jet are weaker. However, its proximity to the wall causes the jet to draw in boundary-layer fluid for

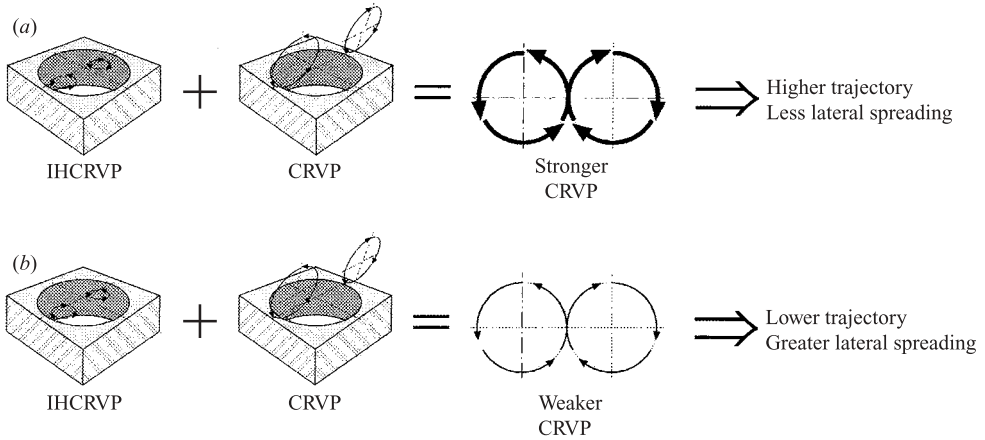


FIGURE 21. CRVP evolution mechanism. (a) coflow configuration. (b) counterflow configuration.

a much greater distance downstream, up to a $0.5D$ increase in the counterflow supply channel case. The effect of wall-proximity due to jet trajectory is further corroborated when comparing the co- and counterflow supply channel results.

Supply channel feed direction is arguably the most interesting of the parameters investigated in this study. The current PIV study not only agrees with the assessments of several previous studies regarding the importance of supply channel feed direction, but also provides detailed velocity fields elucidating the development of the JICF emanating from the short holes.

Hale *et al.* (1999*a,b*; 2000*a,b*) reported that the supply channel feed direction affects both trajectory and spanwise spreading, similar to blowing ratio. Furthermore, they reported that the coflow supply channel geometry was associated with increased trajectory and decreased spanwise spreading when combined with the short injection hole. The current study corroborates that, indeed, the coflow geometry has a much greater trajectory, up to 35% in the case of a blowing ratio of 1.0, and decreased lateral spreading. The increase in trajectory is, in part, due to the greater strength and coherence of the CRVP in the coflow supply channel configuration. In-hole velocity and vorticity data reveal that the coflow supply channel configuration has strong in-hole vortices that enhance the CRVP (because they have the same sense of rotation), thus inducing higher trajectories. The highly coherent CRVP imposes strong effects on the wall near the hole (such as lifting of the boundary-layer fluid downstream of the injection hole), but forces the jet to lift shortly downstream of the injection hole. Hence, the streamwise extent of the CRVP influence is limited.

On the other hand, the counterflow supply channel spawns weaker in-hole vortices, and in the case of the blowing ratio of 0.5, they rotate with opposite rotational sense to the CRVP, destructively interfering with the CRVP and hence creating a much weaker and less coherent CRVP. The weaker vortex-pair remains close to the wall and thus has noticeable effects on the boundary-layer farther downstream of the injection hole than its coflow counterpart. The counterflow supply channel case is associated with an increased length of the recirculation zone downstream of the holes as well, because the jet remains closer to the wall. The CRVP interaction with in-hole structures is summarized schematically in figure 21 for both supply channel configurations.

These detailed velocity field data have enhanced the understanding of the physics of formation of the ubiquitous kidney-shaped CRVP and have revealed how the jet trajectory and evolution are closely linked to the details of the jet development in the supply channel and throughout the short L/D hole.

S. D. P. wishes to acknowledge an Ingersoll–Rand Fellowship.

REFERENCES

- ANDREOPOULOS, J. 1985 On the structure of jets in a crossflow. *J. Fluid Mech.* **157**, 163–197.
- ANDREOPOULOS, J. & RODI, W. 1984 Experimental investigation of jets in a crossflow. *J. Fluid Mech.* **138**, 93–127.
- BECKER, H. A. & MASSARO, T. A. 1968 Vortex evolution in a round jet. *J. Fluid Mech.* **31**, 435–448.
- BOYCE, W. E. & DiPRIMA, R. C. 1997 *Elementary Differential Equations and Boundary Value Problems*, 6th edn. John Wiley.
- BRIZZI, L. E., FOUCAULT, E., BERNARD, A. & BOUSGARBIES, J. L. 1997 In the vicinity of a jet in a cross-flow. FEDSM97-3083, June 1997, CD-ROM.
- BROADWELL, J. E. & BREIDENTHAL, R. E. 1984 Structure and mixing of a transverse jet in incompressible flow. *J. Fluid Mech.* **148**, 405–412.
- BRUNDAGE, A. L., PLESNIAK, M. W. & RAMADHYANI, S. 1999 Influence of coolant feed direction and hole length on film cooling jet velocity profiles. *ASME 99-GT-35*.
- BURD, S. & SIMON, T. 1998 Measurements in film cooling flows: hole L/D and turbulence intensity effects. *ASME J. Turbomach.* **120**, 791–798.
- CATER, J. & SORIA, J. 2001 PIV measurements of turbulent jets. 4th Intl Symp. on Particle Image Velocimetry, Göttingen, Germany, p. 1019.
- CHANG, H. C. 1942 Aufrollung Eines Zylindrischen Strahles Durch Querwind. Doctoral Dissertation, Univ. of Gottingen, 1942; English translation: The roll-up of a cylindrical jet in a crossflow, by K. S. Nagaraja & H. O. Schrade. USAF-ARL 73-0131, Sept. 1973.
- COLLADAY, R. S. & RUSSELL, L. M. 1976 Streakline flow visualization of discrete hole film cooling with normal, slanted, and compound angle injection. *NASA TN D-8248*.
- CRABB, D., DURAO, D. F. G. & WHITELAW, J. H. 1981 A round jet normal to a crossflow. *J. Fluids Engng* **103**, 142–153.
- CUSANO, D. M. & PLESNIAK, M. W. 1999 Asymmetry in a confined rectangular jet in crossflow. *Proc. of Turbulence and Shear Flow Phenomena* (ed. S. Banerjee & J. K. Eaton), Santa Barbara, CA, Paper No. 1-242.
- DRING, R. P. 1982 Sizing criteria for laser anemometry particles. *J. Fluids Engng* **104**, 15–17.
- FOSS, J. 1980 Interaction region phenomena for the jet in a cross-flow problem. *Rep. SFB 80/E/161*, University of Karlsruhe.
- FRIC, T. F. & ROSHKO, A. 1989 Structure in the near field of the transverse jet. *Seventh Symp. on Turbulent Shear Flows, Stanford University, 21–23 August*.
- FRIC, T. F. & ROSHKO, A. 1994 Vortical structure in the wake of a transverse jet. *J. Fluid Mech.* **279**, 1–47.
- GORDIER, R. L. 1959 Studies of fluid jets discharging into moving liquid. St Anthony Falls Hydrodynamics Lab., University of Minnesota, *Tech. Paper* 28, ser. B.
- HALE, C. A. 1999 An experimental and numerical study of the hydrodynamics and surface heat transfer associated with short film cooling holes fed by a narrow plenum. PhD thesis, Purdue University.
- HALE, C. A., PLESNIAK, M. W. & RAMADHYANI, S. 2000a Film cooling effectiveness for short holes fed by a narrow plenum. *ASME J. Turbomach.* **122**, 553–557.
- HALE, C. A., PLESNIAK, M. W. & RAMADHYANI, S. 2000b Structural features and surface heat transfer associated with a row of short-hole jets in crossflow. *Intl J. Heat Fluid Flow* **21**, 542–553.
- HALE, C. A., PLESNIAK, M. W. & RAMADHYANI, S. 1999a Structural features and surface heat transfer associated with a row of short-hole jets in crossflow. *Proc. of Turbulence and Shear Flow Phenomena* (ed. S. Banerjee & J. K. Eaton), Santa Barbara, CA, pp.691–696.

- HALE, C. A., RAMADHYANI, S. & PLESNIAK, M. W. 1999*b* Film cooling effectiveness predictions for short holes fed by a narrow plenum. *ASME IGTI Turbo Expo 99*, Indianapolis, IN, paper no. 99-GT-162.
- HASSELBRINK, E. F. & MUNGAL, M. G. 2001*a* Transverse jets and jet flames. Part 1. Scaling laws for strong transverse jets. *J. Fluid Mech.* **443**, 1–25.
- HASSELBRINK, E. F. & MUNGAL, M. G. 2001*b* Transverse jets and jet flames. Part 2. Velocity and OH field imaging. *J. Fluid Mech.* **443**, 27–68.
- HOLDEMAN, J. D. 1993 Mixing of multiple jets with a confined subsonic crossflow. *Energy Combust. Sci.* **19**, 31–70.
- JOHNSTON, J. P. & KHAN, Z. 1997 The origins of the dominant vortex from a pitched and skewed jet. Paper 1201 (session keynote lecture), *Intl Conf. on Fluids Engng, JSME*, Tokyo, 13–16 July.
- JOHNSTON, J. P., MOSIER, B. P. & KHAN, Z. U. 2001 Effects of inlet conditions on skewed and pitched jets in cross-flow. *2nd Intl Symp. on Turbulent Shear Flow Phenomena*, Stockholm, 27–29 June.
- KAMOTANI, Y. & GREBER, I. 1972 Experiments on a turbulent jet in a cross-flow. *AIAA J.* **10**, 1425–1429.
- KELSO, R. M., LIM, T. T. & PERRY, A. E. 1996 An experimental study of round jets in cross-flow. *J. Fluid Mech.* **306**, 111–144.
- KELSO, R. M. & SMITS, A. J. 1995 Horseshoe vortex systems resulting from the interaction between a laminar boundary layer and a transverse jet. *Phys. Fluids* **7**, 153–158.
- KHAN, Z. U. & JOHNSTON, J. P. 2000 On vortex generating jets. *Intl J. Heat Fluid Flow* **21**, 505–511.
- KOHLI, A. & THOLE, K. A. 1997 A CFD investigation on the effect of entrance flow conditions in discrete film cooling holes. *ASME Proc. 32nd Natl Heat Transfer Conf.* **12**, 223–232.
- KROTHAPALLI, A., LOURENCO, L. & BUCHLIN, J. M. 1990 Separated flow upstream of a jet in a crossflow. *AIAA J.* **28**, 414–420.
- KUZO, D. M. 1996 An experimental study of the turbulent transverse jet. PhD thesis, California Institute of Technology.
- LEBROCQ, P. V., LAUNDER, B. E. & PRIDDIN, C. H. 1973 Experiments on transpiration cooling. *Proc. I MechE* **187**, 149–157.
- LEMMON, C. A., KOHLI, A. & THOLE, K. A. 1999 Formation of counter-rotating vortices in film-cooling flows. *ASME Paper 99-GT-161*.
- LEYLEK, J. H. & ZERKLE, R. D. 1994 Discrete-jet film cooling: a comparison of computations results with experiments. *ASME J. Turbomach.* **116**, 358–368.
- LOEHRKE, R. I. & NAGIB, H. M. 1976 Control of free-stream turbulence by means of honeycombs: a balance between suppression and generation. *J. Fluids Engng* **98**, 342–353.
- MCGOVERN, K. T. & LEYLEK, J. H. 2000 A detailed analysis of film-cooling physics. Part II. Compound-angle injection with cylindrical holes. *ASME J. Turbomach.* **122**, 113–121.
- MARGASON, R. J. 1969 Analysis of the flow field of a jet in a subsonic crosswind. In *Analytic Methods in Aircraft Aerodynamics*, NASA SP 228, 683–702.
- MARGASON, R. J. 1993 Fifty years of jet in cross-flow research. *AGARD-CP 534*, 1–41.
- MOFFAT, R. 1988 Describing the uncertainties in experimental results. *Exps. Therm. Fluid Sci.* **1**, 3–17.
- MORTON, B. R. & IBBETSON, A. 1996 Jets deflected in a crossflow. *Exps. Therm. Fluid Sci.* **12**, 112–133.
- MOUSSA, Z. M., TRISCHKA, J. W. & ESKINAZI, S. 1977 The near field in the mixing of a round jet with a cross-stream. *J. Fluid Mech.* **80**, 49–80.
- PETERSON, S. D. 2001 Experimental investigation of multiple jets in crossflow. MSME thesis, Purdue University, School of Mechanical Engineering.
- PETERSON, S. D. & PLESNIAK, M. W. 2002 Short-hole jet-in-crossflow velocity field and its relationship to film-cooling performance. *Exps. Fluids* **33**, 889–898.
- PIETRZYK, J. R., BOGARD, D. G. & CRAWFORD, M. E. 1989 Hydrodynamic measurements of jets in crossflow for gas turbine film cooling applications. *ASME J. Turbomach.* **111**, 1139–1145.
- PLESNIAK, M. W. & CUSANO, D. M. 2003 Scalar mixing in a confined rectangular jet in crossflow. *J. Fluid Mech.* (submitted).
- RAFFEL, M., WILLERT, C. & KOMPENHANS, J. 1998 *Particle Image Velocimetry: A Practical Guide*. Springer.
- ROBINSON, S. K. 1991 Coherent motions in a turbulent boundary layer. *Annu. Rev. Fluid Mech.* **23**, 601–639.

- RUDMAN, M. 1996 Simulation of the near field of a jet in a cross flow. *Exps. Therm. Fluid Sci.* **12**, 134–141.
- SAMIMY, M. & LELE, S. K. 1991 Motion of particles with inertia in a compressible free shear flow. *Phys. Fluids A* **3**, 1915–1923.
- SHERIF, S. A. & PLETCHER, R. H. 1990 The physical and thermal characteristics of the subsonic jet in a cross stream – a review. *Mixed Convection Environ. Flows* **152**, 83–94.
- SMITH, S. H. & MUNGAL, M. G. 1998 Mixing, structure and scaling of the jet in crossflow. *J. Fluid Mech.* **357**, 83–122.
- THOLE, K. A., GRITSCH, M., SCHULZ, A. & WITTIG, S. 1996 Flowfield measurements for cooling holes with expanded exits. *ASME Paper* 96-GT-174.
- THOLE, K. A., GRITSCH, M., SCHULZ, A. & WITTIG, S. 1997 Effect of a crossflow at the entrance to a film-cooling hole. *J. Fluids Engng* **119**, 533–540.
- UZOL, O. & CAMCI, C. 2001 The effect of sample size, turbulence intensity and the velocity field on the experimental accuracy of ensemble averaged PIV measurements. *4th Intl Symp. on Particle Image Velocimetry, Göttingen, Germany*, P. 1096.
- WALTERS, D. K. & LEYLEK, J. H. 2000 A detailed analysis of film-cooling physics. Part I. Streamwise injection with cylindrical holes. *ASME J. Turbomach.* **122**, 102–112.
- WITTIG, S., SCHULZ, A., GRITSCH, M. & THOLE, K. A. 1996 Transonic film-cooling investigations: effects of hole shapes and orientations. *ASME Paper* 96-GT-222.
- WOLOCHUK, M. C., PLESNIAK, M. W. & BRAUN, J. E. 1994 Evaluation of vortex shedding flow meters for HVAC applications. *Purdue University Rep.* ME-TSPC/HERL-TR-94-1.
- WOLOCHUK M. C., PLESNIAK, M. W. & BRAUN, J. E. 1996 The effects of turbulence and unsteadiness on vortex shedding from sharp-edged bluff bodies. *J. Fluids Engng* **118**, 18–25.
- YUAN, L. L., STREET, R. L. & FERZIGER, J. H. 1999 Large-eddy simulations of a round jet in crossflow. *J. Fluid Mech.* **379**, 71–104.